https://doi.org/10.5194/egusphere-2026-2329
Preprint. Discussion started: 5 May 2026

When the fjords take a breath: Influence of wind forcing and Ekman dynamics on deep ventilation in the North Patagonian fjords

Camila Sola-Hidalgo[1,2,3], Iván Pérez-Santos[2,4*], Manuel I. Castillo[3,6], Marcela Cornejo[1,5], Angela Baldrich[4], Maibelin Castillo-Alvarez[7,8]

[1] Programa de Magíster en Oceanografía, Universidad de Valparaíso y Pontificia Universidad Católica
[2] Centro de Investigación Oceanográfica COPAS COASTAL, Universidad de Concepción, Concepción, Chile
[3] Laboratorio de Oceanografía Física y Satelital (LOFiSat), Universidad de Valparaíso, Valparaíso, Chile
[4] Centro I~mar, Universidad de Los Lagos, Puerto Montt, Chile
[5] Escuela de Ciencias del Mar, Pontificia Universidad Católica de Valparaíso, Valparaíso, Chile
[6] Centro de Observación y Análisis del Océano Costero (COSTAR-UV), Valparaíso, Chile
[7] Postgraduate Program in Oceanography, Department of Oceanography, Faculty of Natural Sciences and Oceanography Universidad de Concepción, Chile
[8] Millennium Institute of Oceanography (IMO), Universidad de Concepción, Chile

Correspondence to: Iván Pérez-Santos (ivan.perez@ulagos.cl)

Abstract. Climate change directly alters the dissolved oxygen (DO) dynamics in the ocean. Ocean ventilation is critical for redistributing nutrients and gases throughout the water column, supporting essential biogeochemical cycles, and regulating the ocean capacity to absorb carbon dioxide and heat, making it essential for climate regulation. In the northern Patagonian fjords, ventilation events mitigate the impacts of deoxygenation and hypoxia, which are primarily driven by the poleward transport of Equatorial Subsurface Water. However, climate-driven changes such as surface warming and increased stratification may reduce the frequency and intensity of these ventilation events, thereby contributing to long-term deoxygenation. In this study, we examined the physical drivers, frequency, and variability of deep ventilation events in the northern Patagonian fjords from 2016 to 2024. ERA5 reanalysis data, from an oceanographic platform moored at 170 m depth, were used to evaluate wind stress, Ekman transport, pumping, and layer depth, alongside in situ time series of temperature, salinity, density, and DO. The results showed a seasonal increase in DO concentrations, classified as ventilation periods, whereas synoptic-scale oxygen events were identified and quantified as ventilation pulses. In total, 16 ventilation periods and 35 pulses were registered over the time series. Onshore Ekman transport favouring downwelling was identified as the main driver of ventilation periods from the austral winter to spring, accompanied by salinity decreases before and during oxygen increases. Pulses coincided with synoptic events dominated by negative total Ekman transport, driven by northern wind stress, along with concurrent thermohaline changes. Overall, these findings provide novel insights into the mechanisms governing oxygen renewal in the Patagonian fjords and underscore the importance of sustained observation systems in a changing ocean.

https://doi.org/10.5194/egusphere-2026-2329
Preprint. Discussion started: 5 May 2026

1 Introduction

Deep ventilation is the process by which "young" surface waters, which are recently exposed to the atmosphere, are injected into the ocean interior, resulting in renewal of properties such as temperature, salinity, and dissolved gas concentrations (Naveira Garabato et al., 2017; Rhein et al., 2017). Ventilation facilitates the downward transport of surface waters, thereby redistributing heat, gases, and nutrients between the surface and ocean interior (Bertrand et al., 2015; Schneider et al., 2017). Such exchange contributes to climate regulation by influencing the capacity of the ocean to store heat and absorb carbon dioxide (de Boer et al., 2007; Yamamoto et al., 2015). In temperate and subpolar regions, deep ventilation is highly seasonal and selective, traditionally associated with deepening of the mixed layer during late winter (Stommel, 1979; MacGilchrist et al., 2021). However, in complex coastal systems such as fjords, this renewal can be asynchronous, with deeper layers responding to different seasonal windows than those of the surface layers (Pinilla et al., 2020). Wind stress and Ekman dynamics are primary physical engines driving transport and convergence at coastal boundaries (Jacox et al., 2018; Klymak et al., 2025); however, other factors such as tidal mixing, deep convection, and dense water overflows play critical roles depending on the local bathymetry and stratification (Font et al., 2024; (Hannah et al., 2024).

With global warming, sea-surface temperatures rise, dissolved oxygen (DO) solubility decreases, and ocean ventilation weakens (Yamamoto et al., 2015; Schmidtko et al., 2017; Shepherd et al., 2017; Breitburg et al., 2018; Palter et al., 2018). Warming enhances stratification and eutrophication, thus reducing vertical oxygen transport, altering biological production and remineralization rates, and ultimately promoting oxygen depletion in marine environments (Keeling et al., 2010; Oschlies et al., 2018). Despite increasing attention to ocean deoxygenation, the physical processes driving deep ventilation and regulating its variability remain poorly understood, limiting our ability to anticipate how the ocean will response to ongoing environmental change. Considering the complexity of DO dynamics, which are shaped by interactions among biological, chemical, geological, and physical factors across spatial and temporal scales, understanding the physical drivers of ventilation is essential for assessing the resilience of marine systems in a warming climate (Zhang et al., 2010; Naveira-Garabato et al., 2017; Levin et al., 2019), the main motivation of the present manuscript.

In the Eastern South Pacific region (ESP), along the Peru–Chile coast, the oxygen minimum zone (OMZ) gradually diminishes in size and intensity as it approaches the Patagonian fjord system (Fuenzalida et al., 2009; Paulmier and Ruiz-Pino, 2009; Silva et al., 2009). The Equatorial Subsurface Water (ESSW) mass is responsible for the OMZ along the southern coasts (Montes et al., 2010). Recent studies have demonstrated the poleward transport of hypoxic (<30 % oxygen saturation, 2 mL L^{-1} or 89.2 µmol L^{-1}) and low-dissolved oxygen waters (LDOW, 30 %–60 % oxygen saturation) within the ESSW, extending into the Patagonian region (Linford et al., 2024). The ESSW carries oxygen-poor, high-nitrate, and elevated-salinity waters into the northern Patagonian fjords, particularly between 43.5° and 45° S, where they enter through the Guafo mouth (GM) (Linford et al., 2023). During winter, water column ventilation increases the deep DO concentrations owing to seasonal hydrographic changes and atmospheric forces. For example, in 2016, complete vertical mixing was observed in the Guafo region, which was attributed to the presence of Subantarctic Surface Water (SAAW) and the influence

https://doi.org/10.5194/egusphere-2026-2329
Preprint. Discussion started: 5 May 2026

of the El Niño event (Buchan et al., 2021; Linford et al., 2023). The El Niño–Southern Oscillation (ENSO) can modulate ventilation by altering wind regimes and water mass transport. El Niño tends to enhance oxygen renewal by deepening the low-oxygen water along the coast through along-coast wave propagation, thus leaving space for oxygenated SAAW, whereas La Niña typically reinforces stratification and inhibits mixing (Henley et al., 2015; Buchan et al., 2021; Linford et al., 2023). However, in 2016, the event was also influenced by intense westerly winds and low-pressure systems that favoured downwelling (Talley, 2011; Aguirre et al., 2012; Rahn and Garreaud, 2014; Saldías et al., 2019), suggesting that surface forcing is critical to deep DO variability (Narváez et al., 2019; Pérez-Santos et al., 2019).

In 2015, Pérez-Santos (2017) reported, for the first time, a deep ventilation event in a Patagonian fjord, which was linked to the inflow of Modified Subantarctic Surface Water (MSAAW) to the Puyuhuapi Fjord (Fig. 1). This ventilation event brought slightly higher DO levels and warmer temperatures, underscoring the dynamic nature of ventilation in these systems. Although Puyuhuapi Fjord experiences persistent hypoxia, DO levels remain above anoxic conditions, suggesting the existence of underlying mechanisms that periodically promote ventilation in the North Patagonian fjords. This ventilation process is crucial for mitigating oxygen depletion and includes molecular diffusion, double-diffusive layering, and external forcing mechanisms such as tides and wind-induced mixing (Talley, 2011; Radko, 2013; Pérez-Santos et al., 2014; Buchan et al., 2021). Molecular diffusion allows the gradual movement of oxygen from higher to lower concentration zones, a slow yet fundamental mechanism in low-energy environments. In contrast, double-diffusive layering arises from temperature and salinity gradients, creating stratified layers that can either hinder or enhance vertical mixing, depending on the local conditions (Radko, 2013; Pérez-Santos et al., 2014). In fjord systems, the interplay of these internal processes with external turbulence sources, such as tidal currents and wind-driven mixing, can trigger episodic deep ventilation events, renew subsurface water properties, and impact biogeochemical cycles (Garreaud et al., 2009; Pérez-Santos et al., 2015; Buchan et al., 2021; Linford et al., 2024; Ross et al., 2025).

With its unique fjord ecosystems, North Patagonia represents a critical but increasingly threatened region, as rising human activities exacerbate oceanic oxygen depletion (Bianchi et al., 2020). Previous studies in this region have largely focused on the causes and consequences of deoxygenation; in contrast, our research will explore the occurrence, frequency, and drivers of deep ventilation processes in the northern Patagonian fjords.

Understanding ventilation processes during ongoing deoxygenation is essential because they directly influence DO dynamics and ecosystem health (Breitburg et al., 2018). The present research provides a mechanistic framework for determining how atmospheric forcing modulates deep ventilation in Patagonian fjords. To address the current knowledge gaps, we analyzed a high-resolution time series (2016–2024) from the GM oceanographic platform (Fig. 1c). The in situ records were complemented using ERA5 reanalysis data to derive key atmospheric variables, including wind stress, Ekman transport, and Ekman pumping. This integration allowed an assessment of how wind-driven dynamics influence vertical mixing and deep ventilation in northern Patagonian fjords. To characterize the nature of ventilation, in this study, we employed a dual conceptual framework evaluating episodic 'Pulses', transient supply events identified via apparent oxygen utilization (AOU) trends, and sustained 'Periods' representing structural oxygenated states. The resulting analysis evaluated the strength and

https://doi.org/10.5194/egusphere-2026-2329
Preprint. Discussion started: 5 May 2026

nature of the physical mechanisms driving ventilation, offering critical insights into the interplay between atmospheric forcing and hydrographic preconditioning.

2. Methodology

2.1. Study area

The study focuses on the northern Patagonian fjords, specifically GM, which serves as the main oceanic gateway between the southern east Pacific Ocean with the interior fjord systems of northern Chilean Patagonia (Fig. 1). The region is characterized by a wide and deep cross-shelf channel of approximately 40 km in width and reaching depths exceeding 250 m, with a U-shaped bathymetric profile (Fig. 1c) that favours the exchange of water masses between the open ocean and fjord network (Ross et al., 2025). Unlike other fjord entrances with pronounced sills or constrictions, the open morphology of GM enables relatively unimpeded advection of subsurface oceanic waters into the Corcovado Gulf and its adjacent channels. These regions are interconnected by narrow channels and shallow sills, which constrain both vertical and horizontal transport of water masses (Silva and Vargas, 2014; Linford et al., 2023). Coupled with substantial freshwater input from rivers and glacial runoff, these topographic features maintain strong salinity-driven stratification, thereby limiting vertical mixing and potentially restricting the downward transport of oxygenated surface waters (Iriarte et al., 2014; Pérez-Santos et al., 2018). In this hydrographic context, GM is pivotal for regulating deep water renewal and oxygen dynamics across the northern Patagonian fjords.

https://doi.org/10.5194/egusphere-2026-2329
Preprint. Discussion started: 5 May 2026

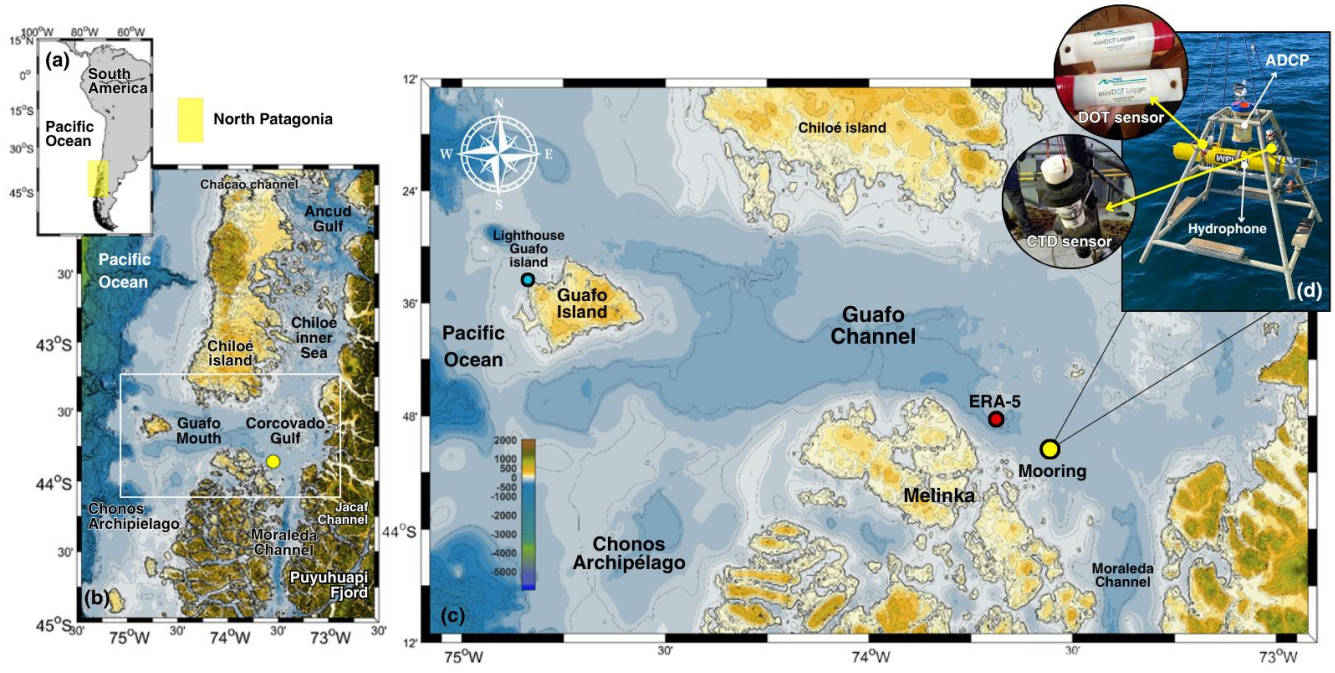

Figure 1. (a) Study area and (b) location of the oceanographic mooring at Guafo Mouth (43°57′ S, 73°40′ W). (c) The mooring system was deployed at approximately 175 m depth. (d) It was equipped with a MiniDOT dissolved oxygen (DO) logger and an RBR dual-channel conductivity–temperature logger installed between 170 and 174 m. These instruments recorded hourly data from January 2016 to December 2024, capturing the variability in DO, temperature, and salinity.

The regional hydrography is primarily governed by the convergence of three oceanic water masses (e.g., SAAW, MSAAW, and ESSW). SAAW, originating in the Southern Ocean and advected northward, typically exhibits salinities between 33.0 and 33.8 g kg^{-1} and high oxygen concentrations (200.67 ± 43.02 µmol L^{-1}), serving as a vital ventilation source for the system (Sievers and Silva, 2008; Crawford et al., 2021). Once inside the fjords, SAAW mixes with continental freshwater to form MSAAW, the most dominant water mass within the interior channels (31–33 g kg^{-1}) (Sievers and Silva, 2008; Pérez-Santos et al., 2014; Linford et al., 2024). In contrast, ESSW is transported southward by the Peru–Chile Undercurrent (PCUC) with typical velocities of 10–50 cm s^{-1} and a core centred at 150–200 m (Hormazábal et al., 2006; Montes et al., 2010). Characterized by salinities >33.8 g kg^{-1} and low DO (89–134 µmol L^{-1}), ESSW is the primary driver of subsurface hypoxia and recent deoxygenation trends in the region (Leth et al., 2004; Linford et al., 2023).

The SAAW and ESSW penetrate towards the fjord system via GM and propagate southward along the Corcovado Gulf, influencing the water-column structure and DO concentrations within the interior basins. From the Gulf, these waters are routed through the Moraleda and Jacaf channels and eventually reach the Puyuhuapi Fjord, while modulating the physical structure and biogeochemical properties of the water column along their trajectory (Schneider et al., 2014; Silva and Vargas,

https://doi.org/10.5194/egusphere-2026-2329
Preprint. Discussion started: 5 May 2026

2014; Pérez-Santos et al., 2018). Historical and recent surveys have documented hypoxic conditions with DO concentrations below 60 μmol L^{-1} at depths >200 m in several fjords within the region, including the Puyuhuapi Fjord, Jacaf Channel, and Aysén Fjord (Silva, 2008; Schneider et al., 2014; Silva and Vargas, 2014; Pérez-Santos et al., 2018; Pinilla et al., 2020; Linford et al., 2023, 2024).

Subtidal circulation at the GM is predominantly two-layered, with a surface outflow toward the ocean and a compensatory bottom inflow to the fjord system. The intensity and direction of these flows exhibit seasonal and sub-seasonal variability, which is regulated by the interplay between barotropic and baroclinic pressure gradients. During the austral winter, elevated freshwater discharge and sea level differences between oceanic and inland regions enhance the barotropic component, favouring persistent near-bottom inflows. In contrast, during the austral summer, weaker barotropic forcing and increased stratification lead to alternating the deeper inflow-outflow patterns, which are modulated primarily by baroclinic dynamics (Ross et al., 2025). Additionally, intraseasonal atmospheric variability modulates flow reversals by generating coastal trapped waves that influence regional sea levels and pressure gradients. Dominant periodicities in the order of 23–30 and 40–70 d have been associated with large-scale climatic oscillations such as the Baroclinic Annular Mode (BAM) and Madden–Julian Oscillation (MJO), which propagate signals into the south eastern Pacific and impact the ocean–fjord exchange (Ross et al., 2025).

The strategic position of the oceanographic platform in the GM makes it a critical location for assessing the deep-water renewal dynamics in northern Patagonia (Fig. 1c). Along with serving as the primary conduit for subsurface oceanic water masses, its variability has been shown to influence fjordic systems that are farther inland. Linford et al. (2023) reported a strong correlation (R^2 = 0.65) between the deep DO time series at the GM and within the Puyuhuapi Fjord, with a temporal lag of approximately 13 d, suggesting that the LDOW entering through GM requires approximately 10 d to reach the interior basins. This temporal and spatial coherence supports the hypothesis that the GM acts as a sentinel zone for tracking the propagation of oceanic DO anomalies into the Patagonian fjord network. Despite its relevance, the mechanisms regulating deep ventilation and oxygen variability in this region remain poorly documented, underscoring the need for focused investigations such as the present study.

2.2. Time series of temperature, salinity, and DO

A mooring system was deployed at GM (43°57′ S, 73°40′ W), at an average depth of ~170 m, and equipped with DO and conductivity–temperature sensors positioned between 170 and 174 m. This site was selected to monitor the variability of deep-oxygen conditions and ventilation processes in the northern Patagonian fjord system (Fig. 1c).

All instruments were configured to record the data at an hourly temporal resolution. The datasets were subsequently averaged to a daily resolution for reducing high-frequency variability (e.g., semidiurnal tides) and ensuring consistency with the temporal scales of the synoptic, intraseasonal, seasonal, and interannual time-scale analyses. DO was recorded using a MiniDOT optical oxygen logger (PME; https://www.pme.com/products/minidot), whereas temperature and conductivity were obtained using an RBR dual-channel logger (RBR Ltd.; https://rbr-global.com/products/standard-loggers/rbrvirtuoso).

https://doi.org/10.5194/egusphere-2026-2329
Preprint. Discussion started: 5 May 2026

The resulting dataset spans from January 2016 to December 2024, providing a nearly continuous multi-year record of the deep-water properties at GM.

Raw conductivity and temperature data were processed according to the Thermodynamic Equation of Seawater 2010 (TEOS-10; McDougall et al., 2009). Practical salinity (SP) was converted to absolute salinity (SA, g kg^{-1}), and in situ temperature was converted to conservative temperature (CT, °C) using the Gibbs SeaWater (GSW) Oceanographic Toolbox for MATLAB. Potential density anomaly (σ_0, kg m^{-3}), referenced to 0 dbar, was calculated from SA and CT and used as a diagnostic variable to characterize water-mass variability and stratification at depth. Oxygen saturation (%) was calculated from the ratio between the observed DO concentration (µmol L^{-1}) and the corresponding equilibrium oxygen concentration at the same temperature and salinity conditions, according to the TEOS-10 formulations. Oxygen saturation was used as a metric complementary to absolute DO for assessing relative oxygenation levels and long-term variability at depth.

The maintenance process of the DO-CT time series of the GM was performed approximately every 6 months, during which the batteries were changed, and CTDO profiles were analyzed to compare with the last record of the time series. Additionally, in 2016, Winkler samples were collected seasonally along the water column. This experiment was repeated in October 2022 (Linford et al., 2023). Comparison between the iodometric titration (the Winkler method) samples and the DO time series of the GM showed good agreement with a correlation coefficient of 0.97, and a centred root mean squared difference (RMSD) of 11.2 µmol L^{-1}.

2.3 Identification of ventilation periods and ventilation pulses

Deep ventilation at the GM was identified using a physically based framework developed in the present manuscript to distinguish transient oxygen supply events from sustained changes in the oxygenation state of the system. At the mooring depth (170 m), net primary production is negligible, and the balance between physical oxygen supply and possible community respiration primarily governs DO variability. Consequently, any sustained increase in DO must be attributed to physical transport processes, such as advection or vertical mixing, rather than to in situ biological production.

Two complementary metrics were defined to capture this dual nature of deep ventilation: (i) ventilated periods, representing sustained intervals (major to 7 d) of enhanced oxygenation, and (ii) ventilation pulses, representing discrete and intense oxygen supply events (between 2 and 7 d). This distinction allows the separation of short-lived physical forcing from longer-lasting oxygenated states in the deep water column, a conceptual framework commonly adopted in studies on fjord and shelf ventilation.

2.3.1 Pre-processing and temporal filtering

Hourly time series of DO, CT, SA, oxygen saturation, and AOU were first processed to remove high-frequency tidal variability. In stratified fjord systems, vertical oscillations of isopycnals (isopycnal heave) can induce large apparent fluctuations in scalar properties at fixed depths, masking the signal of true ventilation processes (Long et al., 2016).

https://doi.org/10.5194/egusphere-2026-2329
Preprint. Discussion started: 5 May 2026

To isolate the subtidal signal relevant to deep ventilation, all hourly variables underwent low-pass filtration using a cosine–Lanczos filter with a cutoff period of 48 hours. This filtering approach has been widely applied in Patagonian fjords to suppress diurnal and semidiurnal tidal variability while retaining the synoptic and intraseasonal dynamics linked to wind forcing and large-scale atmospheric modes (Pinilla et al., 2020; Linford et al., 2024). By removing tidal variability, the filtered series emphasizes the physical processes operating at timescales capable of driving deep renewal, such as wind-driven circulation, barotropic adjustment, and variability associated with regional atmospheric forcing (Pérez-Santos et al., 2019).

After filtering, all variables were averaged to a daily resolution. This additional smoothing step reduces residual high-frequency noise. It aligns the temporal scale of the analysis with that of documented ventilation and inflow events in fjord systems, which typically persist for several days.

2.3.2 Definition of ventilated periods

Ventilated periods were defined as sustained intervals during which deep waters remained both ecologically oxic and anomalously oxygenated relative to the typical conditions in each year. First, a fixed oxygen threshold of 89 μmol L^{-1} (≈2 mL L^{-1}) was applied as a necessary condition. This value corresponds to the regional hypoxia threshold commonly used in studies on Patagonian fjords and the southeastern Pacific margin, ensuring that the identified periods represent oxygen conditions above biologically stressful levels (Silva et al., 2009; Linford et al., 2023). However, the long-term record (2016–2025) includes years with pronounced interannual anomalies, particularly during 2016–2017, which showed substantially elevated background oxygen levels. Using a single global threshold would therefore bias detection toward extreme years and obscure the ventilation signals observed during climatically more typical years. To avoid this effect, a year-specific robust oxygen threshold was computed for each calendar year.

For each year, the median daily DO concentration was calculated as a robust measure of central tendency. Variability was quantified using the median absolute deviation, which is less sensitive to outliers and skewed distributions than that of the standard deviation. The median absolute deviation was then converted to a robust estimate of the standard deviation by multiplying with 1.4826, a scaling factor that ensures equivalence with the standard deviation for normally distributed data (Leys et al., 2013). The year-specific threshold was then defined as the median plus a fraction (k = 0.5) of this robust variability estimate.

The parameter k controls the strictness of the threshold. Sensitivity tests demonstrated that higher values restricted detection almost exclusively to interannual extremes, whereas lower values permitted marginal fluctuations to be classified as ventilated states. The selected value balanced selectivity and representativeness, ensuring detection of physically meaningful anomalies across years of contrasting background conditions.

Finally, a ventilated period was identified during which the daily DO concentrations simultaneously exceeded both the fixed hypoxia threshold (89 μmol L^{-1}) and the year-specific robust threshold for at least 7 consecutive days (1 week). The persistence requirement excludes short-lived fluctuations and ensures that the identified periods represent a genuine shift in

https://doi.org/10.5194/egusphere-2026-2329
Preprint. Discussion started: 5 May 2026

the oxygenation state of the deep layer. The persistence thresholds of this magnitude are consistent with definitions of inflow events in fjord systems, where sustained forcing over several days is required to renew deep waters (Jackson et al., 2025), and with criteria used to define extreme oceanographic events such as marine heatwaves, which require a minimum multi-day duration to exclude short-term meteorological variability (Hobday et al., 2016).

2.3.3 Post-detection consolidation of ventilated periods

Threshold-based detection methods can artificially fragment physically continuous ventilation episodes upon short-lived decreases below the threshold. In deep fjord systems, oxygenation states often fluctuate around the detection threshold owing to residual internal variability, isopycnal heave, or brief relaxation of atmospheric forcing, without necessarily implying termination of the renewal process. To avoid over-segmentation, consecutive ventilated periods separated by short gaps of ≤7 d were merged into a single consolidated episode. This consolidation criterion was chosen to retain consistency with the minimum persistence requirement used for initial detection, thereby preserving methodological symmetry.

The physical justification for this step lies in the characteristic timescales of synoptic wind forcing and deep renewal in the Patagonian fjords. Wind-driven circulation events capable of renewing deep waters typically operate on multi-day to weekly scales (Pérez-Santos et al., 2019; Jackson et al., 2025). Brief interruptions in oxygen concentrations during sustained renewal episodes may reflect transient stratification adjustments, internal variability, or partial relaxation of forcing rather than a true cessation of ventilation. Internal variability in oceanic oxygen fields is known to generate fluctuations comparable with externally forced signals (Long et al., 2016), further supporting the need for preventing the artificial fragmentation of renewal episodes. Importantly, the consolidation step does not modify detection thresholds, introduce new events, or alter the original identification criteria. It simply reorganizes temporally adjacent ventilated states into physically coherent ventilation episodes. This ensures that reported durations reflect meaningful physical processes rather than statistical discontinuities.

2.3.4 Definition of ventilation pulses

Ventilation pulses were defined as strong, short-lived oxygen-supply events capable of initiating or reinforcing ventilatory periods. To distinguish true physical oxygen inputs from temperature-dependent solubility effects, pulse detection was based on AOU rather than DO alone. AOU was calculated as the difference between oxygen saturation and observed DO, with oxygen saturation estimated based on in situ temperature, salinity, and pressure using TEOS-10 (GSW) formulations. At depth, decreases in AOU indicate the arrival of water masses with more recent atmospheric contact or a reduced integrated respiratory history, making AOU a robust tracer of physical ventilation processes (Keeling et al., 2010). Daily AOU tendencies were computed as first differences of the filtered daily AOU series. Only negative tendencies, which correspond to oxygen supply events, were considered. To isolate strong ventilation pulses, a statistical extreme threshold was applied: pulses were identified when the daily decrease in AOU exceeded the mean of all negative AOU tendencies minus two standard deviations of those tendencies. The use of a 2σ criterion follows the established oceanographic practice for identifying strong renewal events and has been applied, for example, by Belzile et al. (2016) in the Saguenay Fjord. This

https://doi.org/10.5194/egusphere-2026-2329
Preprint. Discussion started: 5 May 2026

threshold ensures that the detected pulses represent exceptional oxygen injections rather than background variability, biological noise, or instrumental uncertainty.

Pulses were required to persist for at least 2 consecutive days of decreasing AOU to eliminate isolated single-day anomalies while retaining dynamically meaningful supply events. Further, each pulse was required to achieve oxic success, defined as reaching DO concentrations ≥89 μmol L^{-1} either during the pulse or within a 2 d post-event window and less than 7 d proposed to the ventilation periods (Sect. 2.3.2).

2.4 Atmospheric forcing and wind-derived variables

Surface wind and sea level atmospheric pressure data were obtained from the ERA5 reanalysis (Bell et al., 2020) for the period 2016–2024, with an hourly temporal resolution and a regular spatial grid of 0.25° × 0.25° (https://cds.climate.copernicus.eu/datasets/reanalysis-era5-single-levels). ERA5 provides a reliable representation of atmospheric variability at synoptic and longer time scales in southern Chile. In particular, Pérez-Santos et al. (2019) reported the highest statistically significant correlations between ERA5 surface winds and in situ meteorological observations from the OMARE oceanographic buoy installed in Reloncaví Sound and a Navy lighthouse operating along the outer coastal line of the Patagonian fjords.

2.4.1 Wind stress

The zonal (τ_x) and meridional (τ_y) components of wind stress were calculated using the bulk aerodynamic formulation:

$$\tau u = \rho_a\, C_d\, uU_{10};\ \tau v = \rho_a\, C_d\, vU_{10} \quad (1)$$

where ρa is air density (1.2 kg m^{-3}); C_d is a dimensionless drag coefficient; u and v are the zonal and meridional wind components, respectively; and $U_{10} = \sqrt{u2 + v2}$ is the magnitude of the wind vector at 10 m above sea level.

The drag coefficient C_d was calculated using the formula proposed by Yelland and Taylor (1996), wherein the coefficient varies as a function of wind velocity, according to the following equations:

$$C_d = 0.29 + \frac{3.1}{U_{10}} + \frac{7.7}{U_{10}^2} \times 10^{-3}, for\ U_{10} \le 6\ ms^{-1} \quad (2)$$

$$C_d = 0.60 + 0.07U_{10} \times 10^{-3}, for\ 6\ ms^{-1} \le U_{10} \le 26 ms^{-1} \quad (3)$$

Hourly wind stress fields were subsequently averaged to daily values to match the temporal resolution of the oceanographic analyses.

2.4.2 Ekman dynamics and upwelling indices

Wind-driven horizontal and vertical oceanic responses were quantified using Ekman transport and Ekman pumping (W_E) formulations. The surface Ekman transport components (Ue, Ve; $m^2\ s^{-1}$) were calculated from the daily wind stress as follows:

https://doi.org/10.5194/egusphere-2026-2329
Preprint. Discussion started: 5 May 2026

$$M = \frac{\tau}{\rho_\omega f} \quad (4)$$

where $\rho\omega$ is the seawater density (1025 kg m $^{-3}$), and f is the latitude-dependent Coriolis parameter (which varies as a function of latitude).

W_E (m s^{-1}) was calculated according to Smith (1968), derived from the wind stress curl to evaluate vertical advection:

$$W_E = \frac{1}{\rho\omega f} \nabla \times \tau \quad (5)$$

where $\nabla \times \tau$ is the vertical component of the wind stress curl, which was derived by first-order cross-differencing the wind stress field; this implies that no curl computation was possible for grid points that were the nearest to the coast. This drawback was overcome by applying cokriging to the wind stress curl in two dimensions, thereby enabling extrapolation toward the coast (Marcotte, 1991).

The depth of the surface Ekman layer, D_E (units in meters), was calculated as described by Pond and Pickard (1983) for latitudes (θ) outside ±10° from the Equator:

$$D_E = \frac{4.3}{\sqrt{sin\,|\phi|}}\, U_{10} \quad (6)$$

2.4.3 Total Ekman forcing

To characterize the combined wind-driven forcing acting on the coastal ocean, the total Ekman index (E_{total}) was defined as the sum of the effects of coastal Ekman transport and W_E. The zonal Ekman transport (U_e) was projected onto the cross-shore direction, adopting a sign convention wherein positive values correspond to upwelling-favourable conditions:

$$Ue, \text{coast} = -Ue \quad (7)$$

The W_E velocity was converted to a transport-equivalent term by multiplying W_E by a characteristic horizontal length scale L = 50 km, thus yielding a volumetric flux per unit coastline length. The length scale L was chosen to represent the characteristic width of the continental shelf and the nearshore Ekman response in the Guafo region (Pérez-Santos et al., 2019).

Finally, the total Ekman forcing was defined as follows:

$$E_{total} = Ue, \text{coast} + W_E L \quad (8)$$

expressed in units of m³ s⁻¹ m⁻¹. Positive values indicate wind conditions favourable to upwelling, whereas negative values indicate downwelling-dominated conditions, favouring the ventilation of subsurface waters.

2.5 Statistical and spectral analysis

The annual signal (periods > 250 d) was dominant across all variables, accounting for approximately 70 % of the total variability. As this study focuses on the synoptic-to-intraseasonal variability associated with ventilation processes, the time series were filtered using a Cosine–Lanczos high-pass filter with a half-amplitude cutoff period of 250 d. The DO time series contained several gaps throughout the record. Gaps shorter than 5 d were filled by linear interpolation. Longer gaps were left

https://doi.org/10.5194/egusphere-2026-2329
Preprint. Discussion started: 5 May 2026

unfilled; however, to avoid edge effects during filtering, mirror padding was applied to the boundaries of each gap. This procedure allowed the filtered series to preserve the original temporal coverage while minimizing the artifacts introduced by missing data.

A wavelet analysis was then applied to the high-pass filtered anomalies to examine variability at synoptic, intraseasonal, and seasonal timescales. Continuous Morlet wavelet transforms were used to identify the dominant periodicities, and wavelet coherence analysis was performed to assess the temporal covariance and phase relationship between DO and wind-driven processes. For transparency, the wavelet spectra of the unfiltered DO series are provided in the Supplementary Materials (Fig. S1), demonstrating the dominance of low-frequency variability and supporting the filtering approach adopted here.

A generalized linear model (GLM) with a log-link function and negative binomial distribution (McCullagh and Nelder, 1989) was used to assess the influence of physical predictors on DO variability across the time series. Temperature, salinity, density, and total Ekman transport were included as explanatory variables. Model assumptions were evaluated by testing residual homoscedasticity (Levene test), multicollinearity (variance inflation factor, VIF ≤ 4), and overdispersion (0.75–1.5 range) (Crawley, 2007; Fox and Weisberg, 2010; Venables and Ripley, 2013). Only main effects were considered to avoid overparameterization (Gotelli and Ellison, 2004). Predictor significance was assessed using sequential Type I ANOVA. Model selection was based on the Akaike Information Criterion (AIC) (Akaike, 1974). All analyses were performed in R (R Core Team, 2019) using the packages car, MASS, nlme, lme4, and multicomp.

To further investigate the environmental conditions associated with ventilation pulses, composite analyses were designed around the onset of identified pulse events. Environmental variables were averaged within a ±10 d window relative to the pulse onset, using 35 pulse events. This approach allowed characterization of the typical evolution of wind forcing and the hydrographic conditions before and after the ventilation pulses. Statistical differences between pre-pulse conditions and background variability were evaluated using non-parametric rank-sum tests, and bootstrap resampling was applied to assess the robustness of the observed anomalies. Finally, a principal component analysis (PCA) was performed using the standardized values of DO, Ekman forcing, SA, CT, and potential density during ventilated periods. PCA was used to identify the dominant modes of environmental variability associated with ventilation and to evaluate how pulse days are distributed across the hydrographic–dynamic state space of the system.

3. Results

3.1 Time series dynamics of DO, salinity, temperature, and density

To characterize the temporal variability of DO and associated hydrographic properties at ~170 m depth in GM, we examined the daily time series (2016–2024) together with their monthly climatologies (Fig. 2). The analysis describes the dominant temporal scales and the covariability among oxygen, temperature, salinity, and density.

https://doi.org/10.5194/egusphere-2026-2329
Preprint. Discussion started: 5 May 2026

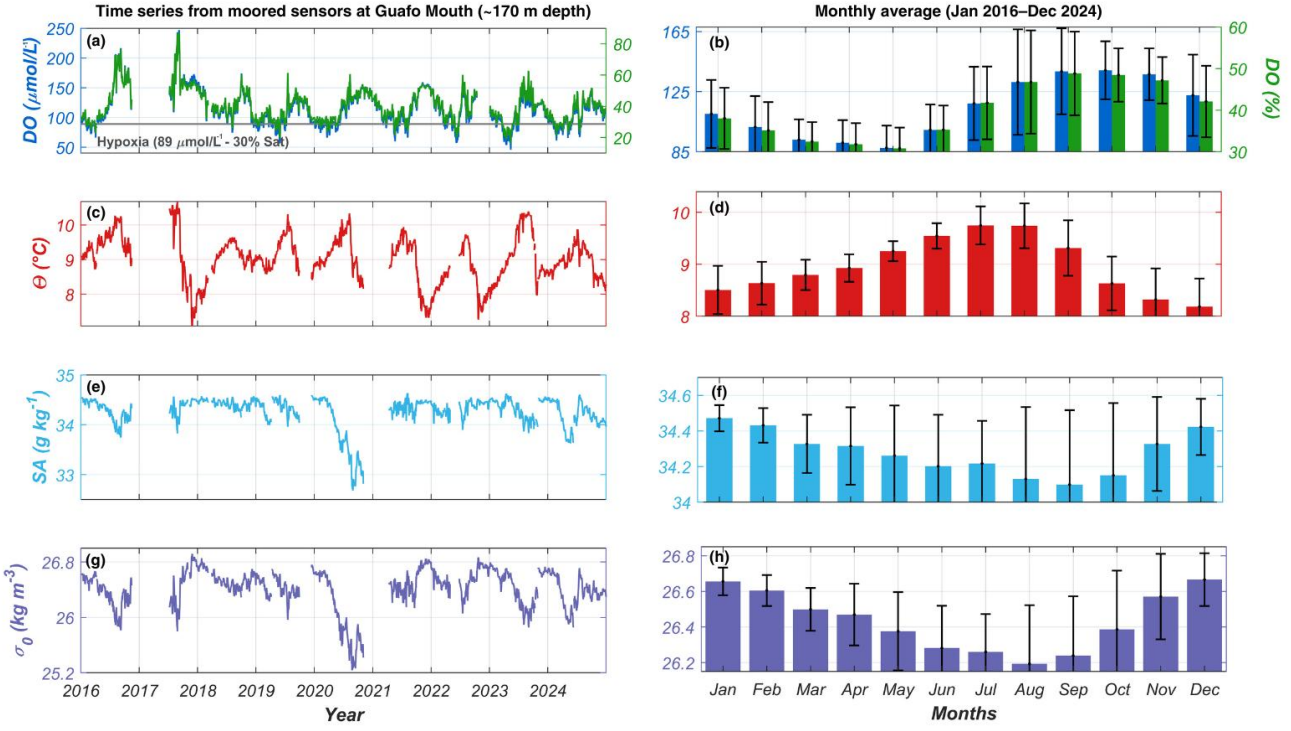

Figure 2. Time series and annual cycles of dissolved oxygen (DO) and hydrographic properties at Guafo Mouth (~170–174 m depth) for the period of January 2016–December 2024. (a) DO (µmol L⁻¹; blue) and oxygen saturation (%; green); the grey horizontal line indicates the hypoxia threshold (89 µmol L⁻¹). (b) Corresponding annual cycle. (c) Conservative temperature (CT, °C; red). (d) Annual cycle of CT. (e) Absolute salinity (SA, g kg⁻¹; light blue). (f) Annual cycle of SA. (g) Potential density anomaly (σ₀, kg m⁻³). (h) Annual cycle of σ₀. All variables were recorded at approximately the same depth and averaged to a daily resolution.

Throughout the time series, the DO ranged between 45 and 246 µmol L⁻¹, with a mean of 114.63 ± 29.23 µmol L⁻¹. The time series revealed strong interannual variability, particularly between 2016–2017, showing sustained high DO, which frequently exceeded 160 µmol L⁻¹ and reached a maximum of 246.76 µmol L⁻¹ in September 2017. After 2018, DO was less variable with seasonal oscillation superimposed to a moderate interannual variability (Fig. 2a). The monthly climatology indicated a well-defined seasonal cycle (Fig. 2b). Mean DO increased in July (117.17 ± 24.45 µmol L⁻¹), reached a peak in October (139.22 ± 19.36 µmol L⁻¹), and remained elevated until November (136.58 ± 17.27 µmol L⁻¹), whereas the lowest monthly mean was observed in May (87.61 ± 14.75 µmol L⁻¹). The seasonal amplitude of the climatological cycle was therefore approximately 51.6 µmol L⁻¹ (Difference between October and May), defining a recurrent ventilation window extending from late winter to late spring (July–November) (Fig. 2b).

The CT ranged from 7.1 to 10.7 °C, with an overall mean of 9.02 ± 0.68 °C (Fig. 2c). The seasonal cycle was evident, with a stronger amplitude (~3 °C at 170 m depth), as observed in the DO time series. Climatologically, the lowest temperatures occurred in December (8.19 ± 0.54 °C) and January (8.51 ± 0.47 °C), whereas the highest monthly mean was recorded in

https://doi.org/10.5194/egusphere-2026-2329
Preprint. Discussion started: 5 May 2026

June (9.55 ± 0.25 °C) and July (9.75 ± 0.37 °C) (Fig. 2d). Several abrupt cooling events were evident from the daily records in late 2017, 2021, and 2022. Importantly, the timing of the minimum temperatures did not coincide with the timing of maximum oxygen concentrations (Fig. 2a and 2c). Oxygen peaked in September–October, whereas the temperature minima occurred in the austral summer (Fig. 2b and 2d). This lack of phase alignment indicated that the seasonal DO maxima was not directly controlled by temperature-driven solubility changes at this depth.

The SA ranged from approximately 32.68 to 34.63 g kg^{-1}, with an overall mean of 34.27 ± 0.31 g kg^{-1}. The climatological cycle showed the minimum SA in September (34.10 ± 0.42 g kg^{-1}) and October (34.15 ± 0.41 g kg^{-1}), coinciding with the period of high DO. The maximum SA was occurred in January (34.47 ± 0.07 g kg^{-1}) and December (34.42 ± 0.16 g kg^{-1}) (Fig. 2f). Further, the σ_0 ranged between 25.24 and 26.92 kg m^{-3}, with a mean value of 26.42 ± 0.28 kg m^{-3} (Fig. 2g). The climatological minimum σ_0 was occurred in August (26.20 ± 0.33 kg m^{-3}) and September (26.24 ± 0.33 kg m^{-3}), whereas the maximum σ_0 was observed in December (26.67 ± 0.15 kg m^{-3}) and January (26.66 ± 0.08 kg m^{-3}) (Fig. 2h). The statistical relationship was supported by ANOVA results (Table S3), which showed that density explains 76.6 % of the variance in DO. These results indicate that oxygen variability at this depth was primarily associated with density variations, which, in turn, are largely controlled by thermohaline variations.

3.2 Ventilation periods and events

The deep DO variability at 170 m in the GM (2016–2024) showed recurrent episodes of rapid oxygen supply (ventilation events) superimposed on longer intervals of sustained oxygenation (ventilated periods) (Fig. 3 and Table 1). The present section scrutinizes both types of DO concentration increases, starting with the longer moments classified as ventilation periods.

https://doi.org/10.5194/egusphere-2026-2329
Preprint. Discussion started: 5 May 2026

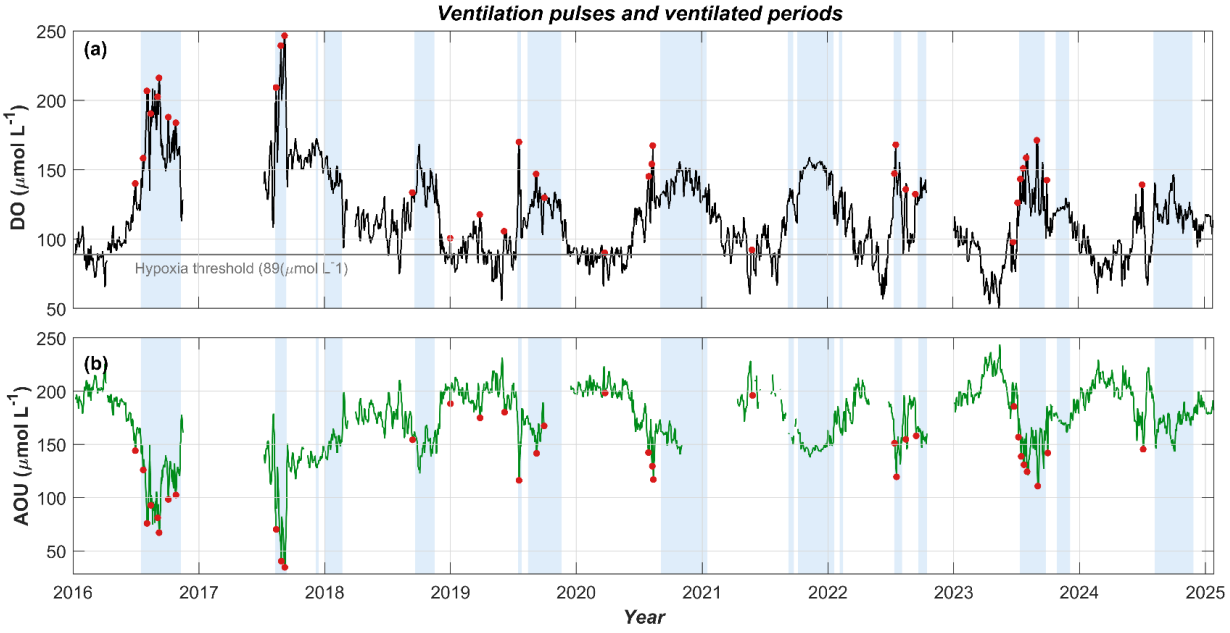

Figure 3. High-resolution time series of (a) dissolved oxygen (DO) and (b) apparent oxygen utilization (AOU, µmol L⁻¹) at ~170 m depth in Guafo Mouth (2016–2024). Light blue shading indicates ventilated periods identified from the filtered daily DO series. Red circles mark ventilation pulses, represented by the local DO maxima in panel (a) and the corresponding AOU minima in panel (b). The horizontal grey line in panel (a) indicates the regional hypoxia threshold (89 µmol L⁻¹).

Table 1. Ventilated periods are defined as intervals during which daily dissolved oxygen (DO) exceeds both the regional hypoxia threshold (89 µmol L⁻¹) and a year-specific robust threshold for ≥7 consecutive days and are grouped if separated by ≤7 d. The reported statistics correspond to daily filtered DO values and include the period duration, mean DO (± standard deviation), and minimum and maximum DO. Ventilation intensity is quantified as ΔAOU, defined as the decrease in apparent oxygen utilization (AOU) from the onset of each period to its minimum value.

ID	Start date	End date	Duration (d)	DO mean ± std (µmol L⁻¹)	DO min (µmol L⁻¹)	DO max (µmol L⁻¹)	ΔAOU (µmol L⁻¹)
1	16-Jul-2016	09-Nov-2016	117	172.00 ± 19.30	131.34	216.12	87.084
2	10-Aug-2017	12-Sep-2017	34	208.15 ± 23.63	154.93	246.57	68.882
3	06-Dec-2017	14-Dec-2017	9	170.02 ± 2.06	166.42	172.75	3.247
4	01-Jan-2018	21-Feb-2018	52	144.93 ± 7.62	132.15	160.13	8.967
5	20-Sep-2018	16-Nov-2018	58	141.35 ± 10.75	122.7	168.56	34.856

https://doi.org/10.5194/egusphere-2026-2329
Preprint. Discussion started: 5 May 2026

6	16-Jul-2019	26-Jul-2019	11	141.70 ± 18.16	122.26	169.96	45.304
7	14-Aug-2019	20-Nov-2019	99	125.67 ± 7.75	102.9	146.94	32.500
8	03-Sep-2020	15-Jan-2021	135	139.05 ± 7.99	121.95	155.9	20.783
9	08-Sep-2021	24-Sep-2021	17	131.25 ± 3.54	125.26	137.03	10.732
10	06-Oct-2021	19-Jan-2022	106	148.79 ± 7.40	125.03	159.17	26.932
11	04-Feb-2022	14-Feb-2022	11	131.59 ± 3.51	124.91	137.72	7.789
12	12-Jul-2022	04-Aug-2022	24	143.81 ± 10.08	129.37	167.99	37.207
13	20-Sep-2022	15-Oct-2022	26	134.20 ± 5.09	125.52	144.81	19.600
14	12-Jul-2023	25-Sep-2023	76	135.30 ± 14.09	116.25	171.18	53.748
15	27-Oct-2023	05-Dec-2023	40	122.58 ± 2.58	118.99	129.65	16.432
16	06-Aug-2024	27-Nov-2024	114	121.92 ± 8.91	103.68	146.56	27.300

3.3. Quantification of the ventilated periods

According to the methodology described in Sect. 2.3, a total of 16 ventilated periods were identified during 2016–2024 (Table 1 and Fig. 3). Period durations ranged from 9 to 135 d, with a median of ~50 d. The longest continuous ventilated interval occurred between 3 September 2020 and 15 January 2021, lasting 135 d, followed by extended periods in July–November 2016 (117 d) and August–November 2024 (114 d). Ventilation periods were not evenly distributed throughout the year. However, all the analyzed years had ventilation periods. (Fig. 3) Most events were initiated during the austral winter to early spring (July–September) and frequently extended into spring or early summer (October–January). Shorter ventilated intervals were also observed in the austral summer (e.g., January–February 2018, 52 d), but these were generally less frequent and shorter than the winter–spring events. Mean DO during the ventilated periods (Table 1) ranged from 121.92 ± 8.91 μmol L^{-1} (Aug–Nov 2024) to 208.15 ± 23.63 μmol L^{-1} (Aug–Sep 2017). The highest ventilated period occurred in August–September 2017, which also exhibited the highest DO of the entire record (246.57 μmol L^{-1}). In contrast, the late-2023 and 2024 periods were characterized by a lower DO (≈122–135 μmol L^{-1}) but remained consistently above the hypoxia threshold. The intra-period variability, expressed as the standard deviation of daily filtered DO, ranged from ±2.58 μmol L^{-1} (Oct–Dec 2023) to ±23.63 μmol L^{-1} (Aug–Sep 2017). Periods with higher DO tended to exhibit greater variability, whereas the lower-mean periods in 2023–2024 were comparatively stable. The minimum DO within the ventilated periods

https://doi.org/10.5194/egusphere-2026-2329
Preprint. Discussion started: 5 May 2026

consistently remained above the regional hypoxia threshold (89 µmol L^{-1}), with the observed minima ranging from 102.9 µmol L^{-1} (Aug–Nov 2019) to 154.93 µmol L^{-1} (Aug–Sep 2017). The maximum DO within the periods varied substantially, from 129.65 µmol L^{-1} (Oct–Dec 2023) to 246.57 µmol L^{-1} (Aug–Sep 2017).

3.4. Quantification of ventilation pulses

This study also marked a difference between the sustained ventilated periods (longer in time) and ventilation pulses (shorter in time). A total of 35 ventilation pulses were identified in the filtered DO time series (Fig. 3; red dots on the black line). Pulses were detected as short-lived oxygenation events characterized by abrupt decreases in AOU and corresponding rapid increases in DO (Fig. 3). The detection criteria identified events in which these changes persisted for at least 2 consecutive days. Ventilation pulses represent episodic oxygen-replenishment events that do not necessarily evolve into sustained ventilated periods. Their temporal distribution relative to the ventilated periods revealed two main configurations: pulses occurring both in and out of the ventilated periods. Several pulses occurred within the ventilated periods, often appearing in clusters. This behaviour was particularly evident in Period 1, i.e., during winter 2016 (from July to November), and in Period 14, during winter 2023 (from July to September), where multiple pulses were distributed throughout the ventilated interval. These clusters suggest that sustained ventilated conditions may result from the accumulation of several episodic oxygenation events occurring over consecutive weeks. Intense pulses in August 2017 were observed at the period with the highest mean and maximum DO. Here, the pulse reached ~246 µmol L^{-1} (2017), whereas in more recent years (2022–2024) it was generally moderate, at below ~170 µmol L^{-1}.

In other cases, ventilated periods were closely associated with individual pulses. For example, Period 5 and Period 6 were characterized by short ventilation intervals coinciding with isolated pulses, indicating that brief oxygenation events can occasionally produce short-lived ventilated conditions. Several pulses were also identified outside the ventilated periods, representing isolated oxygenation events that did not lead to sustained ventilation. These outsider pulses typically correspond to brief increases in oxygen that rapidly return to the background conditions. Overall, the coexistence of clustered pulses within ventilated periods and isolated pulses outside them highlights the episodic character of deep oxygen renewal at the GM, where sustained ventilation may emerge from the accumulation of multiple short-lived oxygenation events.

3.5. Seasonal patterns of the wind stress and W_E

The long-term seasonal mean of the wind stress showed a clear annual cycle over the GM region (Fig. 4). The meridional component (τ_v) demonstrated a marked seasonal contrast with predominantly northward stress during austral summer–spring (JFM–OND) (Fig. 4a and 4d) and predominantly southward stress during austral autumn–winter (AMJ–JAS) (Fig. 4b and 4c). This seasonal contrast was spatially coherent across the 42–46° S domain and was intensified along the coastal margin. In terms of wind stress intensity, a northward maximum area was observed during austral summer (0.05 N m^{-2}), covering mostly the northern region of the study area (Fig. 4a). In contrast, during austral winter, southward wind stress was the maximum near the shore, particularly inside the Chiloé Inner Sea (CIS) (Fig. 4c).

https://doi.org/10.5194/egusphere-2026-2329
Preprint. Discussion started: 5 May 2026

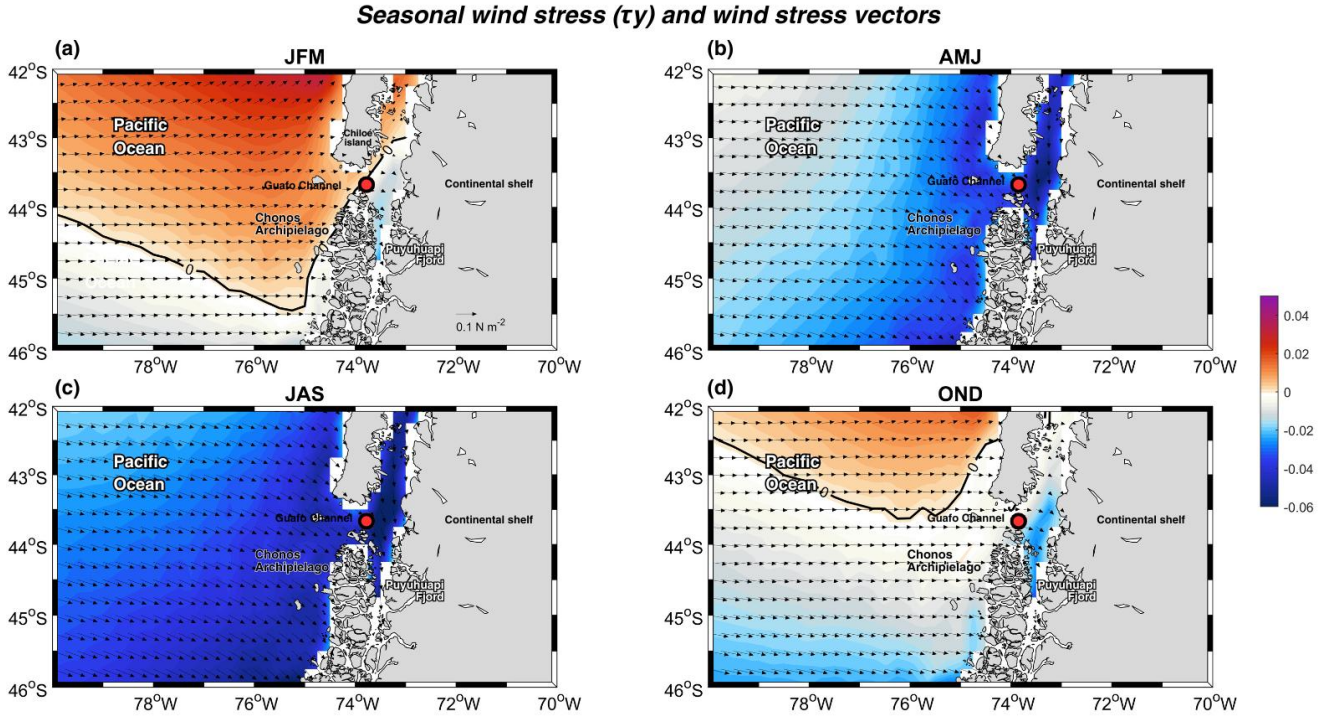

Figure 4. Long-term seasonal mean of meridional wind stress (τy; colour shading, N m⁻²) and wind stress vectors (τx, τy; arrows) for (a) JFM, (b) AMJ, (c) JAS, and (d) OND over the Guafo Mouth region (42–46° S, 70–78° W). Positive τy values indicate northward wind stress, whereas negative values indicate southward wind stress, following the ERA5 convention. Arrows indicate the direction and relative magnitude of wind stress (τx, τy). The red point marks the mooring position.

To understand wind stress variability, a time series was extracted near the mooring site (see Fig. 1c, red dot). The 2016–2024 wind stress time series further illustrated the high-frequency variability superimposed on the seasonal cycle (Fig. 5a and 5c). The zonal wind stress (τ_x) values were mostly positive throughout the record, showing episodic peaks exceeding ±0.30 N m⁻². Furthermore, the long-term monthly mean (Fig. 5b) remained within a relatively narrow range between 0.013 N m⁻² in June and 0.028 N m⁻² in January, indicating a weak seasonality. In contrast, the meridional wind stress (τ_v) displayed a stronger seasonal structure (Fig. 5d). The long-term monthly mean ranged from −0.056 N m⁻² in August to 0.026 N m⁻² in January, yielding a seasonal amplitude of 0.082 N m⁻². Negative values dominated the time series, particularly during austral, autumn, and winter, consistent with downwelling-favourable conditions, whereas the summer months were characterized by near-neutral to slightly positive stress. Standard deviations were the largest during winter months, reflecting enhanced synoptic variability during this period. These results highlight the dominance of the meridional wind-stress component in the seasonal wind-forcing regime in the Guafo region.

https://doi.org/10.5194/egusphere-2026-2329
Preprint. Discussion started: 5 May 2026

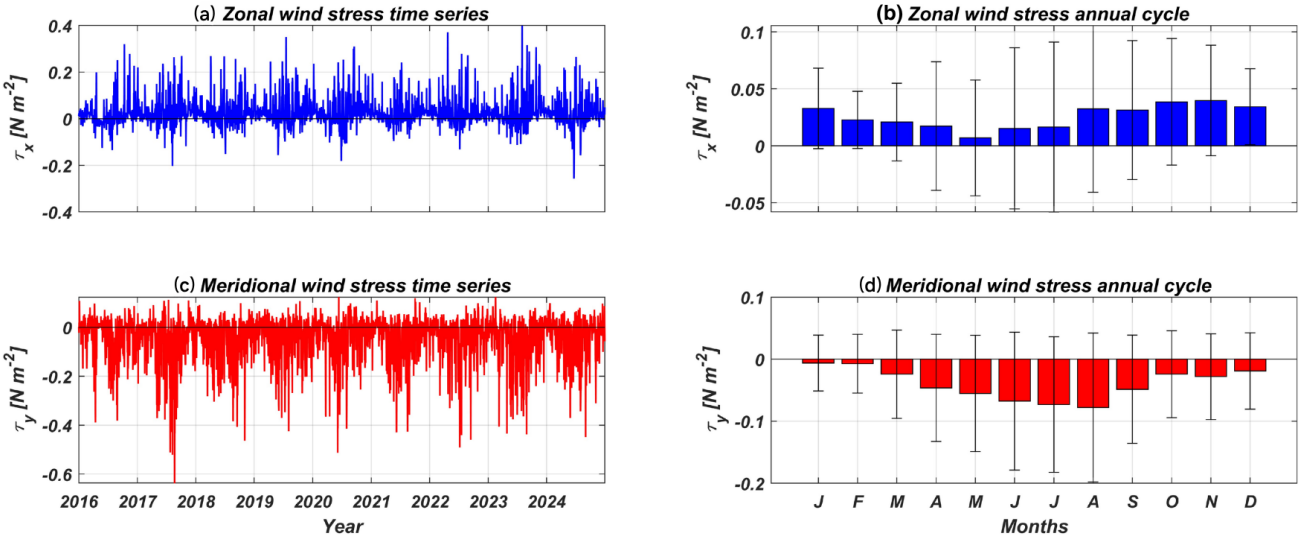

Figure 5. Time series (2016–2024) and annual cycle of wind stress (monthly means ± standard deviation) components and wind energy transfer over the Guafo Mouth region. (a) Zonal wind stress (τx; N m⁻²) time series. (b) Long-term monthly mean cycle of τx. (c) Meridional wind stress (τy; N m⁻²) time series. (d) Long-term monthly mean cycle of τy. Positive τx indicates eastward stress, and positive τy indicates northward stress.

The long-term seasonal mean of the Ekman transport (Fig. 6; black arrows) and W_E (Fig. 6; colour-coded) reveal a well-defined seasonal cycle of Ekman-driven atmospheric circulation over the GM region. In general, northward Ekman transport dominated seasonality. During the austral fall and winter, the Ekman transport slightly shifted towards the northeast (Fig. 6c and 6b), favouring the advection of oceanic water into the Patagonian fjord through the GM and contributing to Ekman-downwelling conditions, as registered by the W_E in the same season (negative in Fig. 6). Moreover, during the austral summer–spring season, Ekman upwelling conditions dominated along the coastal zone (42°–44° S), particularly along the western coast of Chiloé Island and the GM (Fig. 6a and 6d).

https://doi.org/10.5194/egusphere-2026-2329
Preprint. Discussion started: 5 May 2026

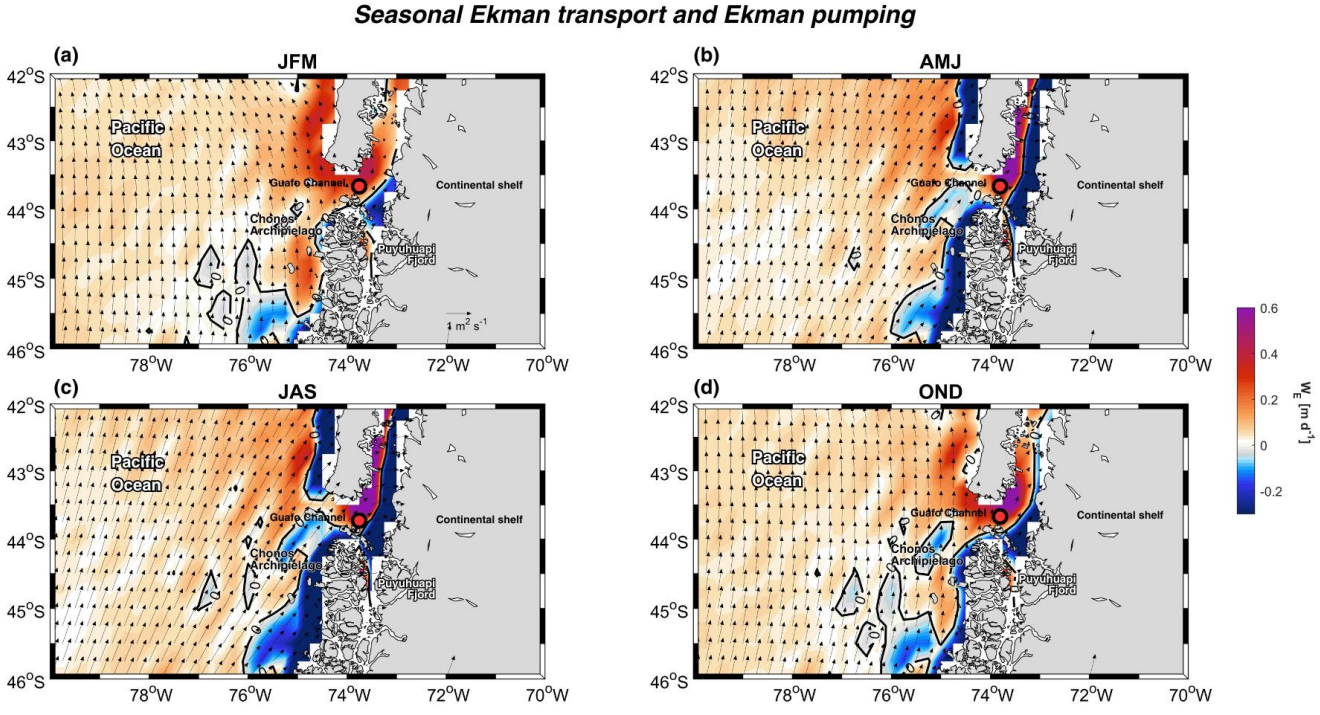

Figure 6. Long-term seasonal mean (2016–2024) of Ekman transport (vectors; m² s⁻¹) and Ekman pumping velocity (W_E; colour shading, m s⁻¹) for (a) JFM, (b) AMJ, (c) JAS, and (d) OND over the Guafo Mouth region (40–47° S). Positive values (warm colours) indicate upward W_E, whereas negative values (cool colours) indicate downward W_E. Arrows represent the direction and relative magnitude of Ekman transport. The red point marks the mooring position.

Using the same wind stress time series dataset, the records were utilized to obtain the Ekman time series of the transport, pumping, and layer depth (Fig. 7). The zonal Ekman transport (U_e), projected onto the cross-shore direction, exhibits a pronounced seasonal maximum during austral winter (Fig. 7a), mainly because of the meridional wind stress patterns (Fig. 5c). The long-term monthly mean ranged from 0.060 m² s⁻¹ in January to 0.754 m² s⁻¹ in August, yielding a seasonal amplitude of 0.693 m² s⁻¹. The largest monthly standard deviation also occurred in August (1.16 m² s⁻¹), indicating enhanced winter variability (Fig. 7b). W_E exhibits a clear seasonal reversal, dominated by negative values, and therefore favouring the Ekman-downwelling (Fig. 7c). After conversion from m s⁻¹ to m d⁻¹, the long-term monthly mean ranged from +0.100 m d⁻¹ in December to −0.250 m d⁻¹ in August, resulting in a seasonal amplitude of 0.351 m d⁻¹. The largest monthly standard deviation occurred in July (0.693 m d⁻¹), reflecting enhanced winter variability in vertical forcing (Fig. 7d). The composite total Ekman forcing (E_total; Fig. 7e), integrating cross-shore transport and pumping contributions, reached its weakest (least negative) monthly mean in January (−0.00353 m³ s⁻¹ m⁻¹) and its strongest (most negative) transport in August (−0.898 m³ s⁻¹ m⁻¹), corresponding to a seasonal amplitude of 0.895 m³ s⁻¹ m⁻¹. The largest standard deviation was again observed in August (1.45 m³ s⁻¹ m⁻¹), indicating that winter conditions maximize both the intensity and variability of coastal convergence

https://doi.org/10.5194/egusphere-2026-2329
Preprint. Discussion started: 5 May 2026

(Fig. 7f). Finally, the D_E showed the absolute maximum exceeding the 80 m depth, highlighting the winter months with the maximum and highest standard deviations (Fig. 7g and 7h). Overall, Ekman transport, pumping, and the composite convergence index all exhibited coherent winter amplification, with August consistently representing the month of maximum magnitude and variability. This seasonal intensification aligns with the dominance of meridional wind stress during austral winter, indicating that Ekman downwelling was favoured.

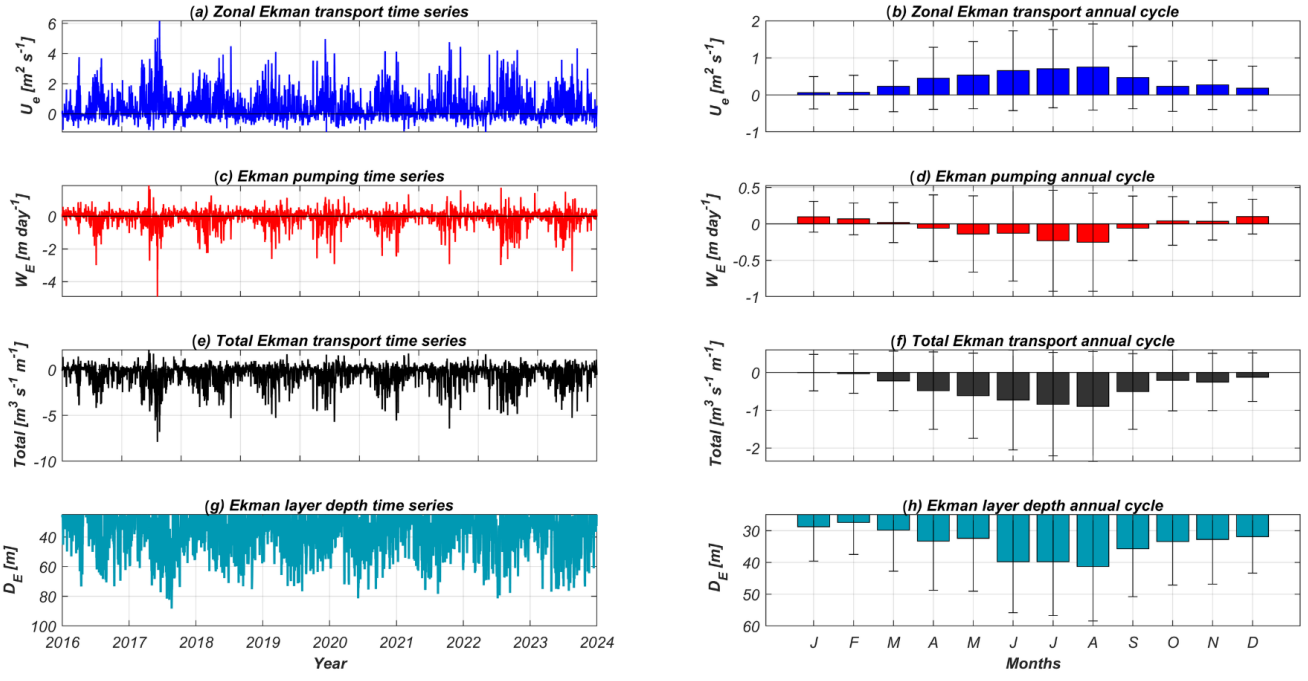

Figure 7. Time series (2016–2024) and annual cycle of Ekman dynamics over the Guafo Mouth region. Time series are shown in the left panels and climatological annual cycles (monthly means ± standard deviation) are shown in the right. (a) Zonal Ekman transport (U_e; m² s⁻¹) time series. (b) Climatological annual cycle of U_e. (c) Ekman pumping velocity (W_E; m d⁻¹) time series. (d) Climatological annual cycle of W_E. (e) Total Ekman transport (m² s⁻¹) time series. (f) Climatological annual cycle of total Ekman transport. (g) Ekman layer depth (D_e; m) time series. (h) Climatological annual cycle of D_e. Positive W_E values indicate upward W_E, whereas negative values indicate downward pumping.

3.6 Wind-driven dynamics and water mass properties during ventilation pulses and ventilation periods

Thermohaline conditions and wind forcing associated with ventilation pulses and ventilated periods were examined using the mean CT, SA, and total Ekman forcing calculated for each event (Fig. 8 and Tables 2 and S2). To further characterize the atmospheric forcing associated with ventilation pulses, composite analyses were constructed relative to the pulse onset (Fig. 8). Downwelling-favourable wind forcing intensified during the days preceding pulse events, as indicated by the increasingly negative Ekman transport and meridional wind stress between approximately −5 and −1 d relative to the pulse onset (Fig.

https://doi.org/10.5194/egusphere-2026-2329
Preprint. Discussion started: 5 May 2026

525 8a–8c). These pre-event wind anomalies were statistically significant compared with those of the background conditions (rank-sum test: $p = 5.85 \times 10^{-6}$ for Ekman transport; $p = 7.24 \times 10^{-6}$ for meridional wind stress; $p = 2.89 \times 10^{-5}$ for W_E). Bootstrap resampling further confirmed that the observed Ekman anomaly preceding pulses was highly unlikely to arise from random variability ($p < 0.001$). Following the pulse onset (day 0), DO increased rapidly by approximately 15–20 µmol L^{-1}, reaching peak values within approximately 1–3 d (Fig. 8d). This oxygenation was followed by a decrease in SA and a
530 low increase in CT, suggesting the arrival of a distinct water mass during the ventilation events (Fig. 8e and 8f).

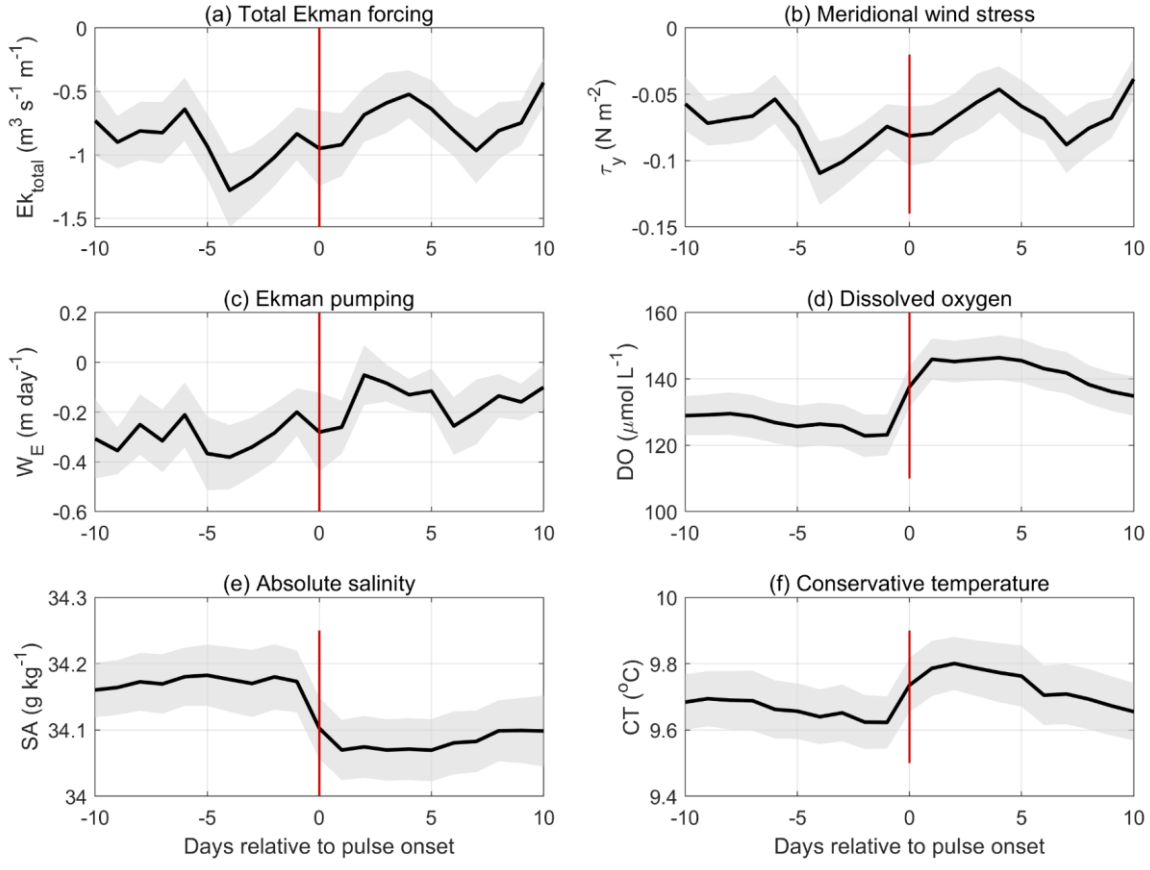

Figure 8. Composite evolution of wind forcing and hydrographic conditions relative to the onset of ventilation pulses at ~170 m depth in the Guafo Mouth region. Solid lines represent the composite mean across 35 ventilation pulses, and the grey shading indicates ±1 standard error of the mean. The vertical red line marks the pulse onset (day 0). Panels show (a) the total Ekman
535 **transport, (b) meridional wind stress (τy), (c) Ekman pumping velocity (W_E), (d) dissolved oxygen (DO), (e) absolute salinity (SA), and (f) conservative temperature (CT). Downwelling-favourable wind forcing intensifies several days before pulse onset, followed by an increase in DO and concurrent changes in hydrographic properties.**

Other ocean-atmosphere processes of the regional scale could also contribute to the observed ventilation pulses. The study
540 region is a corridor of atmospheric rivers (ARs), and ventilation pulse 6 was influenced by the passage of AR in July 2019

https://doi.org/10.5194/egusphere-2026-2329
Preprint. Discussion started: 5 May 2026

(Fig. 9). This event occurred inside the ventilation period 6 (Fig. 9 and Tables 1 and 2). During this interval, the DO concentrations in the water column increased markedly from 80 to 180 µmol L^{-1}. This rise in DO coincided with a strengthening of the wind to 16 m s^{-1} and a wind direction favouring eastward Ekman transport, which resulted in downwelling conditions (Fig. 9a). These combined atmospheric and oceanographic factors facilitated the vertical transport of oxygen-rich surface waters into deeper layers, underscoring their role in driving the ventilation pulses observed during this period. Future investigations should focus on evaluating other synoptic processes, such as the passage of low- and high-pressure systems, which could also favour ventilation pulses.

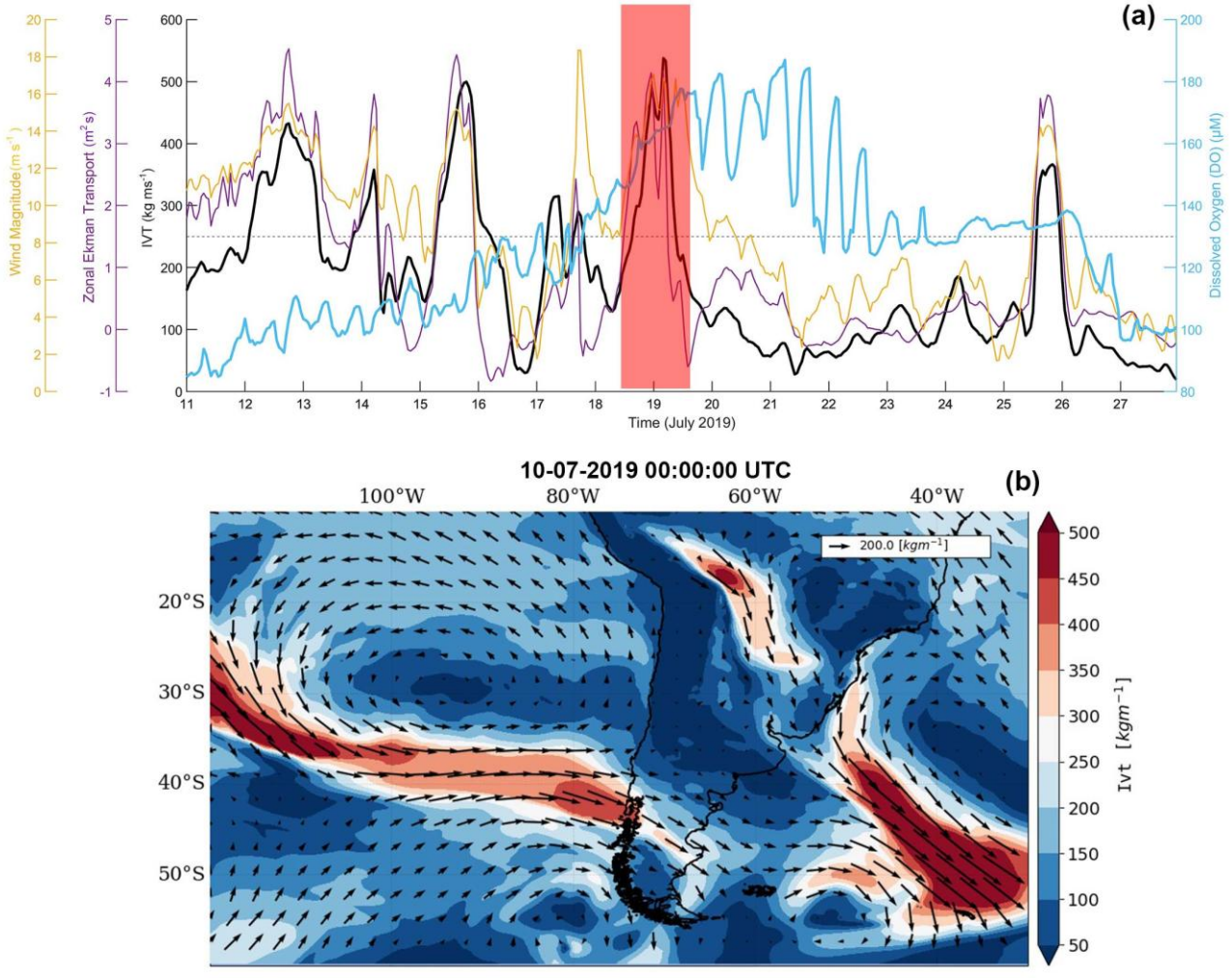

Figure 9. (a) Hourly time series of integrated vapour transport (IVT), with values exceeding 250 kg m^{-1} s^{-1} used to identify the influence of atmospheric rivers (ARs). The panel also displays an hourly time series for dissolved oxygen (DO), zonal Ekman transport (U_e), and wind magnitude. (b) Map depicting the passage of the AR on 19 Jul, 2019. The colour scale indicates IVT values, whereas arrows represent the wind magnitude and direction.

https://doi.org/10.5194/egusphere-2026-2329
Preprint. Discussion started: 5 May 2026

In contrast, ventilated periods exhibited more persistent hydrographic conditions than those of the individual pulses described previously (Table 2). The mean CT and SA values calculated for each ventilated period were relatively stable during sustained ventilation intervals. Across the identified periods, salinity generally remained lower than that of the background conditions. Simultaneously, CT was slightly elevated, consistent with the hydrographic patterns observed during individual pulses but was maintained over longer timescales. Wind forcing averaged over the ventilated periods also indicated conditions generally favourable to downwelling (Table 2), although the magnitude and persistence of Ekman forcing varied between years. In several periods, sustained ventilation coincided with intervals of persistently negative Ekman forcing. The duration of the ventilated periods ranged from several weeks to multiple months, and many intervals contained multiple ventilation pulses, indicating that sustained ventilation frequently comprised sequences of shorter oxygenation events.

Table 2. Ventilated periods are defined as intervals during which daily dissolved oxygen (DO) exceeds both the regional hypoxia threshold (89 µmol L^{-1}) and a year-specific robust threshold for ≥7 consecutive days and are grouped if separated by ≤7 d. The statistics correspond to the daily filtered DO values.

ID	Start date	End date	Duration (d)	DO mean ± std (µmol L^{-1})	CT (°C)	SA (g kg^{-1})	σ (kg m^{-3})	**Ek total (m^3 s^{-1} m^{-1})**
1	16-Jul-2016	09-Nov-2016	117	172.00 ± 19.30	9.710	34.061	26.146	**−0.639**
2	10-Aug-2017	12-Sep-2017	34	208.15 ± 23.63	10.385	34.108	26.069	**−1.689**
3	06-Dec-2017	14-Dec-2017	9	170.02 ± 2.06	7.358	34.503	26.851	**−0.034**
4	01-Jan-2018	21-Feb-2018	52	144.93 ± 7.62	8.024	34.488	26.742	**−0.087**
5	20-Sep-2018	16-Nov-2018	58	141.35 ± 10.75	8.999	34.359	26.492	**−0.458**
6	16-Jul-2019	26-Jul-2019	11	141.70 ± 18.16	10.126	34.082	26.093	**−0.641**
7	14-Aug-2019	20-Nov-2019	99	125.67 ± 7.75	9.078	34.217	26.370	**−0.335**
8	03-Sep-2020	15-Jan-2021	135	139.05 ± 7.99	8.588	33.103	25.580	**−0.194**

https://doi.org/10.5194/egusphere-2026-2329
Preprint. Discussion started: 5 May 2026

9	08-Sep-2021	24-Sep-2021	17	131.25 ± 3.54	9.521	34.181	26.270	**−0.714**
10	06-Oct-2021	19-Jan-2022	106	148.79 ± 7.40	7.776	34.435	26.737	**−0.047**
11	04-Feb-2022	14-Feb-2022	11	131.59 ± 3.51	8.153	34.262	26.547	0.246
12	12-Jul-2022	04-Aug-2022	24	143.81 ± 10.08	9.421	34.101	26.224	**−0.407**
13	20-Sep-2022	15-Oct-2022	26	134.20 ± 5.09	8.610	34.359	26.553	**−0.179**
14	12-Jul-2023	25-Sep-2023	76	135.30 ± 14.09	10.234	34.086	26.077	**−0.964**
15	27-Oct-2023	05-Dec-2023	40	122.58 ± 2.58	8.591	34.426	26.608	**−0.470**
16	06-Aug-2024	27-Nov-2024	114	121.92 ± 8.91	8.913	34.175	26.362	**−0.405**

To further examine the environmental variability associated with ventilated conditions, a PCA was applied to DO, Ekman forcing, SA, CT, and potential density during the ventilated periods (Fig. 10). The first two components explained 71 % of the total variance (PC1: 48.3 %, PC2: 22.7 %). PC1 was primarily associated with hydrographic structure, showing strong positive loadings from SA (0.52) and density (0.61) and negative contributions from CT (−0.47), representing variability in water-mass properties during the ventilated conditions. PC2 was dominated by Ekman forcing (loading = 0.57), reflecting variability in wind-driven circulation. DO projected negatively along PC2 (loading = −0.48), indicating that oxygen variability is closely linked to dynamic forcing conditions. Pulse days tended to cluster toward negative values of PC1 and PC2, suggesting that ventilation pulses occurred under specific hydrographic states and particular wind-forcing conditions.

https://doi.org/10.5194/egusphere-2026-2329
Preprint. Discussion started: 5 May 2026

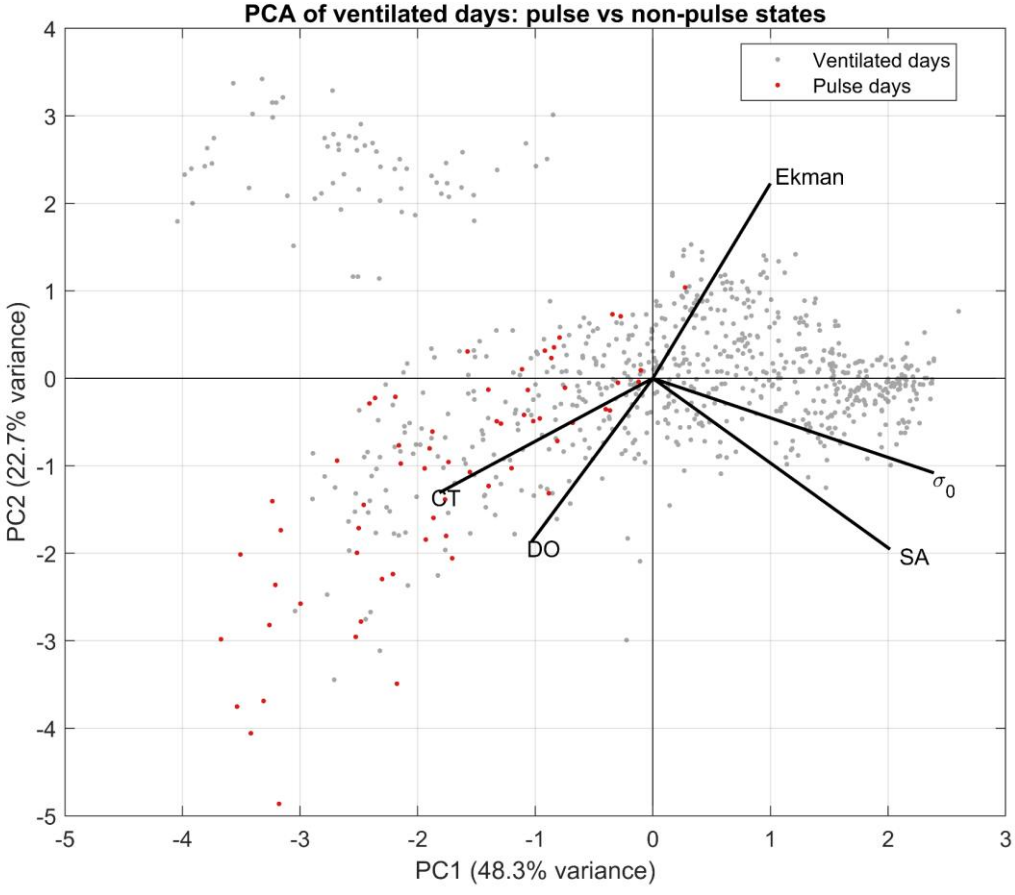

Figure 10. Principal component analysis (PCA) of environmental conditions during the ventilated periods at ~170 m depth in the Guafo Mouth region. Grey points represent the daily observations within ventilated periods, whereas red points indicate days classified as ventilation pulses. Black arrows show the variable loadings. The first two components explain 71 % of the total variance (PC1: 48.3 %; PC2: 22.7 %). PC1 is primarily associated with hydrographic structure, showing strong positive loadings from absolute salinity (SA) and density and negative contributions from conservative temperature (CT). PC2 is dominated by Ekman forcing. Pulse days tend to cluster toward negative values of PC1 and PC2, suggesting that ventilation pulses occur under specific hydrographic states modulated by wind-driven forcing.

3.7 Wavelet and coherence analysis of DO variability

To identify the dominant timescales of DO variability and to assess its dynamical relationship with wind-driven processes, continuous Morlet wavelet analyses were applied to the daily time series. Initial wavelet analyses of the unfiltered DO record revealed that spectral energy was strongly concentrated at periods longer than ~250 d (Fig. S1), indicating dominant sub-annual to interannual variability. Similar low-frequency dominance was observed across all wind-derived variables (not shown), suggesting that variability at periods >250 d accounted for the majority of the total variance in the system. Spectral inspection indicated that this band represented approximately 70 % of the total variance across variables. Because this strong

https://doi.org/10.5194/egusphere-2026-2329
Preprint. Discussion started: 5 May 2026

low-frequency signal masked the higher-frequency variability of interest, a high-pass cosine–Lanczos filter with a 250 d cutoff was applied to isolate synoptic and intraseasonal fluctuations, consistent with the ventilation period and pulses.

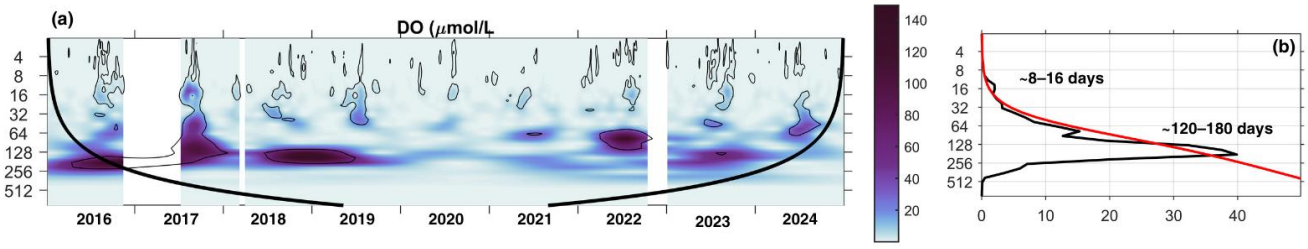

Figure 11. Wavelet analysis of high-pass filtered dissolved oxygen (DO) at ~170 m depth. (a) Wavelet power spectrum showing enhanced variability concentrated at synoptic (8–16 d) and semi-annual (~120–180 d) periods throughout the record. Significant regions (95 % confidence) are enclosed by black contours, and the cone of influence is shown by the thick black curve. (b) Global wavelet spectrum indicating dominant energy peaks within the intraseasonal band. Filtering of low-frequency (>250 d) variability reduces the spectral dominance of interannual signals and enhances the detection of wind-related timescales.

The wavelet power spectrum of the filtered DO series (Fig. 11a) shows two dominant bands. The semi-annual band with periods between 120 d and 250 d and the synoptic variability on a timescale of approximately 8 to 16 d were stronger between 2016 and mid-2019; during this time, the spectral energy was persistent and well-defined. The spectral energy of this band in 2024 was lower than that in 2016–2019. Within this semi-annual band, episodic intensifications around ~100–120 d were also evident. The second dominant band corresponded to synoptic variability on a timescale between 8 and 16 d. In contrast to the semi-annual band, this higher-frequency signal appeared as recurrent, intermittent patches of power distributed throughout most of the time series. Notably, 2017 exhibited enhanced power across a broad range of periods, with strong energy spanning both the synoptic and sub-annual bands. The global wavelet spectrum (Fig. 11b) confirmed that statistically significant power (above the 95 % red-noise threshold) was concentrated primarily in two ranges: 8–16 d and 120–180 d. Simultaneously, the global spectrum indicated the overall significance of these bands, whereas the time–frequency representation demonstrated that the sub-annual band was temporally confined and strong between 2016 and mid-2019 and weaker thereafter. In contrast, synoptic variability persisted intermittently throughout the record.

3.7.1 Wavelet coherence with wind forcing

Wavelet coherence analysis was conducted between filtered DO and all wind-derived variables; the full set of coherence spectra and phase relationships is presented in Fig. S2. Here, the study focused on meridional wind stress (τy) and W_E, which exhibited the strongest and most consistent coherence with DO (Fig. 12). For τ_y/DO coherence (Fig. 12a), strong and significant coherence was observed in the 120–250 d band between 2016 and 2017. This sub-annual coherence weakened substantially from 2018 through late 2022. During this interval, coherence shifted toward shorter periods, with recurrent and significant patches in the 30–60 d range that persisted across much of 2018–2022. From 2023 to 2024, coherence in the 120–250 d band re-emerged, whereas the 30–60 d band remained intermittently significant throughout the record.

https://doi.org/10.5194/egusphere-2026-2329
Preprint. Discussion started: 5 May 2026

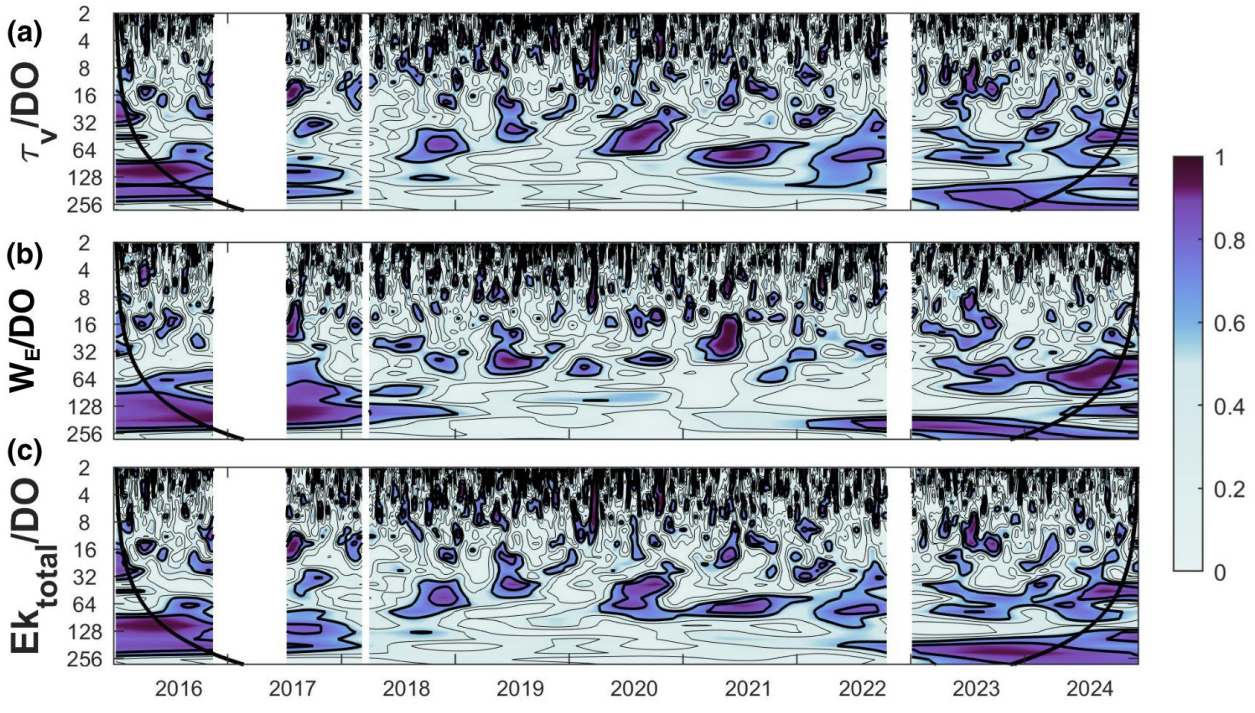

Figure 12. Wavelet coherence between high-pass filtered dissolved oxygen (DO) and wind-derived forcing variables. (a) Meridional wind stress (τy) versus DO. (b) Ekman pumping (W_E) versus DO. (c) Ekman total versus DO. Colours represent the coherence magnitude, black contours denote the 95 % confidence level, and the thick black line indicates the cone of influence. Significant coherence is concentrated within the synoptic and intraseasonal timescales.

A similar pattern was observed for W_E/DO coherence (Fig. 12b). Strong semi-annual coherence (120–250 d) dominated between 2016 and late 2018. This band weakened between 2019 and mid-2022, during which coherence was primarily expressed in the 30–60 d range. From mid-2022 onward, sub-annual coherence reappeared, coexisting with persistent shorter-period coherence patches. Across both τ_y and W_E, synoptic-scale coherence (8–16 d) appeared intermittently throughout the time series but was less temporally continuous than that of the 30–60 d band. The consistency between τy–DO and We–DO coherence patterns indicates that deep oxygen variability was dynamically linked to meridional wind forcing and its associated vertical Ekman response across multiple timescales, with temporal modulation of the dominant coupling frequency (Fig. 12c).

4. Discussion

A time series of DO, together with temperature and salinity records, was used to investigate the variability of DO in the deep layer of the northern Patagonian fjords (Fig. 1). This study was inspired by the recent work of Linford et al. (2023), which

https://doi.org/10.5194/egusphere-2026-2329
Preprint. Discussion started: 5 May 2026

demonstrated marked deoxygenation in the DO time series, but lacked the ability to examine periods with increased DO levels and investigate whether these high DO levels are part of a seasonal cycle or shorter-term events. This gap in knowledge was the focus of this study and its discussion section, which aims to address these overlooked periods of elevated DO.

4.1 Seasonal and synoptic controls on deep ventilation at GM

A novel methodology was applied to the temporal variability of the 170 m DO time series (2016–2024) for identifying ventilation periods, representing the seasonal expression of sustained oxygenation, and ventilation pulses, representing its synoptic-scale expression. The criteria presented in Sect. 2.3 allowed the detection of 16 ventilated periods, with an average duration of 58 ± 43 d (Table 1). The DO record indicated that this variability did not result from random fluctuations but rather reflected a clear seasonal background state on which higher-frequency oxygenation events were superimposed (Figs. 2 and 3). Most ventilated periods occurred during late winter and early spring, when the deep layer transitioned from recurrent hypoxic or low-oxygen conditions to sustained oxic states.

Within this framework, ventilated periods represented sustained oxygenated states of the deep layer, whereas pulses represented discrete oxygen-supply events. This distinction was physically important because elevated DO alone did not necessarily imply active renewal at the time of observation. Including AOU was therefore essential, as ventilation, in the physical sense, implies water renewal rather than simply the maintenance of high oxygen concentrations (Keeling et al., 2010; Ayranci and Dashtgard, 2020). At depth, decreases in AOU indicate the arrival of waters with more recent atmospheric contact or a lower integrated respiratory history, making AOU a more robust tracer of renewal than DO alone (Sarmiento and Gruber, 2006; Silva and Vargas, 2014).

Of the grouped ventilated periods identified at 170 m, most followed a recurrent pattern consistent with the canonical deep-ventilation signal at GM. These periods were generally associated with negative total Ekman forcing, indicating downwelling-favourable conditions (Figs. 4–6), together with increasing DO, decreasing salinity at the mooring, slightly elevated CT, and reduced AOU.

This behaviour was particularly evident for the strongest grouped periods, namely periods 1, 2, 6, 12, 14, and 16 (Tables 1 and 2), and was also observed, although with varying intensity, in periods 5, 7, 8, 13, and 15. In seasonal terms, these periods occurred predominantly between August and November, defining a recurrent winter–spring ventilation window in the 170 m record. Within this window, the combination of downwelling-favourable forcing and local evolution toward fresher, more oxygenated, and slightly warmer conditions represented the dominant mode of sustained deep oxygenation. Downwelling-favourable winds and the resulting oxygenation of deep layers have also been frequently reported in the British Columbia fjords by Jackson et al. (2015, 2022). In this region, intense downwelling winds can ventilate the water column to depths of up to 350 m (Jackson et al., 2025).

However, the case analysis also showed that the seasonal window alone was insufficient to explain the intensity, duration, or renewal efficiency of individual periods. Rather, the period-specific expression depended on the coupling between the

https://doi.org/10.5194/egusphere-2026-2329
Preprint. Discussion started: 5 May 2026

seasonal forcing background and the sequence, magnitude, and persistence of renewal events, as reflected in the local evolution of salinity, temperature, and AOU time series. In particular, periods that developed when salinity at the mooring was already decreasing, or continued to decrease during the period, tended to reach higher oxygen concentrations, exhibit stronger apparent renewal, or persist for longer duration. This point deserves emphasis. The combined role of downwelling-favourable forcing and local water properties does not imply that the vertical structure of the water column can be resolved from the present observations. Instead, it indicates that at the measurement depth, periods associated with fresher conditions are generally more effective at sustaining elevated oxygen. In this sense, salinity at 170 m emerged as an important local factor controlling the strength and persistence of the ventilated state, even if part of this salinity signal was itself linked to the same forcing that promoted renewal.

This distinction is particularly important because grouped ventilated periods were defined from a DO-based criterion (upper hypoxia limit and upper annual media; Sect. 2.3) and not from the AOU. Therefore, some periods formally satisfied the threshold for a ventilated state without necessarily representing substantial deep-water renewal. This was particularly clear for periods 3 and 4, which occurred outside the typical ventilation window, from 6 to 14 December 2017 and from 1 January to 21 February 2018, respectively. In both cases, the AOU suggested little to almost no renewal, while temperatures at 170 m were exceptionally low. These periods are therefore better interpreted as oxygenated states maintained primarily by enhanced oxygen solubility under cooling (Keeling et al., 2010; Gruber, 2011), rather than as true ventilation events in the sense of active renewal. Their occurrence demonstrates that elevated DO alone is insufficient as evidence of ventilation and requires renewal diagnostics to distinguish between physically renewed and thermodynamically sustained oxygenated states.

A second set of atypical cases included periods that likely began under the usual seasonal ventilation regime but remained elevated for reasons that were not fully canonical. Period 8, extending from 3 September 2020 to 15 January 2021, began within the expected winter–spring window and likely originated through the same downwelling-related mechanism as the typical periods. However, its unusually long persistence appears to have been favoured by exceptionally low salinity at 170 m, the lowest of the full record. Period 10, from 6 October 2021 to 19 January 2022, followed a similar seasonal onset but its extended duration was more plausibly associated with unusually low temperatures at the mooring, particularly toward the end of the period. These two cases suggest that some long-lasting periods were initiated under the normal seasonal ventilation framework but were subsequently sustained by local anomalies in salinity or temperature that helped maintain high oxygen concentrations beyond the usual seasonal window (Fig. 2). By contrast, period 11, which occurred in February, showed almost no evidence of renewal, little indication of downwelling-favourable forcing, and only weak AOU support for active ventilation. Rather than reflecting a newly generated renewal episode, this is more plausibly interpreted as the persistence of elevated oxygen inherited from the preceding period.

The interpretation emerging from these observations suggests that although the seasonal cycle established the window of susceptibility, it did not independently determine the renewal strength or persistence. This behaviour is consistent with the pulse-dominated circulation described for the GM, where subtidal exchange is regulated by the interaction between barotropic and baroclinic pressure gradients (Ross et al., 2025). Such a seasonal-to-synoptic organization aligns with global

https://doi.org/10.5194/egusphere-2026-2329
Preprint. Discussion started: 5 May 2026

observations from other semi-enclosed systems, including the Masfjorden in Norway (Sagen et al., 2025), the Strait of Georgia (Ayranci and Dashtgard, 2020), and the Saanich Inlet in Canada (Hamme et al., 2015), where deep-water supply is discontinuous and triggered by short-lived events. Consequently, these findings support a framework wherein deep renewal at the GM is seasonally organized but expressed through discrete episodes rather than a continuous progression (Moffat, 2014; Pérez-Santos et al., 2019; Ross et al., 2025).

The spectral analyses reinforced this multi-scale interpretation, as the wavelet spectrum of the filtered DO record exhibited primary energy concentration in two distinct bands, specifically a synoptic signal at 8–16 d and a broader intraseasonal band centred between 120 and 180 d (Fig. 11). These results aligned with the established scales of atmospheric variability and seasonal cycles in the eastern austral Pacific (Torrence and Compo, 1998; Pérez-Santos et al., 2019). Furthermore, the coherence analyses revealed that the coupling between DO and wind-driven forcing reached its maximum strength in the 120–250 d band during 2016 and 2017, before weakening and shifting toward shorter periodicities between 2018 and 2022. This shift indicates that the deep oxygen variability at the GM was modulated by both intraseasonal and synoptic forcing, with the relative dominance of these drivers undergoing significant interannual changes. Consequently, the seasonal ventilation window emerged as a dynamic feature rather than a static annual occurrence.

Within this framework, Fig. 9 provides a particularly clear example of how a synoptic atmospheric disturbance can operate within the seasonal ventilation window. The July 2019 event occurred during the winter period when downwelling-favourable forcing was already climatologically expected but the AR appeared to have sufficiently intensified the low-pressure-driven forcing to promote a marked oxygenation event. This case, therefore, illustrates how seasonal susceptibility and synoptic amplification can act together: July provided a favourable background, whereas the AR likely intensified the downwelling conditions that sustained the ventilation in that year. Rather than representing a mechanism separate from the winter circulation pattern, the AR can be interpreted as its particularly intense synoptic expression (Garcia-Santos, 2025a, 2025b).

Overall, deep ventilation at GM should considered the result of a seasonal window of opportunity that is intermittently activated and modulated by synoptic forcing, rather than as a purely seasonal or purely event-driven process. The grouped ventilated periods captured the sustained oxygenated expression of that process, but their duration and renewal efficiency depended on whether the seasonal background was reinforced by repeated short-lived oxygen-supply events and whether local thermohaline conditions at 170 m favoured the persistence of oxygenated waters.

4.2 Anatomy of ventilation pulses: Synoptic triggers and active renewal

Ventilation pulses represent an event-scale mechanism. Because pulses were identified from strong negative AOU tendencies, they specifically captured episodes of active renewal rather than merely elevated oxygen concentrations. This distinction is important because, unlike ventilated periods, which may also include oxygenated states maintained by persistence or solubility effects, pulses indicate the discrete arrival of younger, more oxygenated water masses (Ayranci and

https://doi.org/10.5194/egusphere-2026-2329
Preprint. Discussion started: 5 May 2026

Dashtgard, 2020). In this sense, the 35 pulses identified in our record provide the clearest expression of when effective renewal reached 170 m (Table S2).

Despite differences in intensity and context, the pulses followed a coherent general pattern. The composite analysis showed that pulse onset was typically preceded by increasingly negative total Ekman forcing and wind stress from the north during the previous few days, followed by a rapid increase in DO, decline in salinity, slight increase in CT, and decrease in AOU (Fig. 8). This sequence indicates that pulses were recurrent dynamic events associated with downwelling-favourable forcing and the subsequent arrival of relatively fresher, more oxygenated, and slightly warmer waters at 170 m. Thus, although ventilated periods described the intervals during which the deep layer remained oxygenated, pulses identified the discrete renewal events that generated or reinforced these states. Such a lagged sequence indicates that the pulses were not instantaneous responses to local atmospheric cooling but rather resulted from the intrusion or subduction of relatively fresher, warmer Subantarctic-derived waters into the deep layer (Silva and Vargas, 2014). Similar lagged responses between wind forcing and deep oxygenation have been observed in other fjord systems, such as the Juan Perez Sound in Canada, where strong winter winds facilitate the mixing and advection of shelf waters into deep basins (Jackson et al., 2025).

Many pulses occurred within ventilated periods and contributed to their maintenance. In these cases, the relationship between pulses and periods was cumulative rather than one-to-one. Some long periods were not generated by a single dominant renewal event but by a succession of pulses that repeatedly refreshed the deep layer before oxygen depletion could be re-established. This was particularly clear during the longest and most persistent periods, including period 1 in 2016, as well as during later prolonged periods such as those identified in 2023. Under these conditions, pulses served as reinforcing events that sustained an already favourable oxygenated state, maintaining elevated DO for timescales much longer than those of the individual injections. The implication is that persistence at 170 m depended on whether renewal occurred, as well as on how frequently and how closely spaced the renewal events were within the broader ventilation window.

However, a substantial number of pulses also occurred outside grouped ventilated periods. These isolated events show that short-lived oxygen intrusions can occur at almost any time of the year when sufficiently strong downwelling-favourable forcing develops. However, such events rarely evolved into sustained ventilated states outside the main winter–spring ventilation season. In most cases, they remained brief perturbations in the DO record and did not persist long enough to satisfy the period criterion. This suggests that transient forcing alone was insufficient to maintain ventilation at depth. Rather, isolated pulses appeared to represent renewal events that failed to develop into prolonged oxygenation because the forcing relaxed rapidly, because the local thermohaline conditions at 170 m were unfavourable for persistence, or because both factors acted simultaneously (Klymak et al., 2025).

This asymmetry between pulses occurring inside and outside the periods is central for interpreting the ventilation process. A pulse always implied some degree of renewal as embedded in its AOU-based definition. However, renewal was not equivalent to persistence. Some pulses produced substantial oxygen increases without generating a period, whereas others of comparable or even lower apparent intensity helped sustain long oxygenated intervals. The difference lies in the background state onto which the pulse was superimposed. When pulses occurred during the main ventilation season, under lower salinity

https://doi.org/10.5194/egusphere-2026-2329
Preprint. Discussion started: 5 May 2026

and lower density conditions already favourable to oxygenation, they were more likely to sustain ventilated states. When they occurred outside this background state, their signal was usually short-lived.

In this framework, ventilation pulses can be understood as the event-scale building blocks of the deep oxygen cycle at GM. Some were effective enough, or occurred under sufficiently favourable background conditions, to initiate or prolong ventilated periods. Others remained isolated because the forcing did not persist or because the local state of the system did not allow oxygenated waters to remain at depth. Overall, the 35 pulses demonstrate that deep renewal was fundamentally discontinuous: the deep layer was ventilated through a sequence of short-lived oxygen-supply events, but only a subset of these events translated into sustained oxygenated states.

4.3 Interannual variability: Contrasting pathways to ventilation efficiency

Although deep ventilation at GM followed a recurrent winter–spring seasonal pattern, its intensity, duration, and renewal efficiency varied markedly from year to year. This interannual variability was evident in the DO time series at 170 m (Fig. 2), in the duration and characteristics of grouped ventilated periods (Tables 1 and 2), and in the temporal structure of the wavelet and coherence analyses (Figs. 11 and 12). Among all years, 2016 and 2017 stood out as the most ventilated but did not represent the same type of event. Instead, they defined two contrasting expressions of ventilation efficiency: one dominated by persistence and cumulative reinforcement, and the other dominated by intensity.

The 2016 event represented the most persistent ventilation regime of the record. Period 1 lasted 117 d and showed the largest cumulative renewal, sustained by a succession of pulses rather than a single extreme oxygenation event (Fig. 2 and Table 1). In this case, deep oxygenation was maintained through repeated reinforcements that prevented complete re-establishment of oxygen depletion, thus producing a prolonged multi-episodic ventilated state. Therefore, the event stands out for its duration as well as for how this duration was built: through recurrent renewal events that maintained high oxygen levels for several months. The exceptional persistence of this period likely resulted from the synergy between remote climatic forcing and local atmospheric triggers. During the 2015–2016 “El Niño” event, the lower boundary of the oxygen-poor ESSW deepened at the fjord entrance, promoting the intrusion of oxygenated SAAW into the Guafo region (Linford et al., 2023). Simultaneously, El Niño-related atmospheric anomalies displaced the South Pacific Subtropical Anticyclone southward, allowing an intensification of low-pressure systems and downwelling-favourable conditions over northern Patagonia (Pérez-Santos et al., 2019). Consequently, the record-long ventilation from mid-July to early November 2016 reflected the coupling of favourable oceanic preconditioning and recurrent winter forcing, allowing successive renewal events to accumulate into the most persistent ventilated state observed in the 9 year series (Ross et al., 2025).

By contrast, 2017 was characterized by a shorter but more intense ventilation regime. Period 2, between 10 August and 12 September 2017, coincided with the highest DO concentrations of the entire time series and with the strongest downwelling-favourable forcing observed in the record (Fig. 2 and Table 1). Unlike 2016, the exceptional character of 2017 was not the persistence but the intensity and apparent efficiency of the renewal. The strongest pulses of that year were concentrated within a relatively short interval, yet they produced the most extreme oxygenation signal and the lowest AOU values of the

https://doi.org/10.5194/egusphere-2026-2329
Preprint. Discussion started: 5 May 2026

series (Fig. 3b). Thus, 2016 reflected cumulative multi-episodic reinforcement whereas 2017 represented a more concentrated ventilation extreme dominated by intense forcing.

The 2017 ventilation regime demonstrated the dominance of extreme synoptic forcing over the large-scale hydrographic preconditioning observed in previous years. During this period, the system reached its highest recorded DO concentration of 246.57 µmol L^{-1} and the most intense negative total Ekman forcing in the 9 year dataset (Table 2). Unlike the prolonged stability of 2016, ventilation in 2017 was characterized by shorter, more concentrated episodes, during which pulses such as P10 and P11 achieved the maximum renewal efficiency (Table S2). These results suggest that sufficiently intense synoptic triggers can overcome neutral hydrographic conditions to effectively reset the deep layer through vigorous downwelling (Pérez-Santos et al., 2019)

Figure 9 provides an important intermediate example of how interannual variability can also depend on the occurrence of particularly intense synoptic disturbances within the winter ventilation season. The July 2019 atmospheric-river event did not produce a ventilated year comparable to 2016 or 2017 in cumulative terms but clearly illustrated how a strong short-lived atmospheric perturbation can amplify the expected winter downwelling regime and produce a marked oxygenation response at depth. In this sense, Fig. 9 is valuable not as an exceptional interannual outlier but as a process example showing how the strength of embedded synoptic events may contribute to the year-to-year differences in ventilation expression.

Large-scale climate modes further modulated this interannual efficiency by regulating the frequency and intensity of the synoptic triggers. The BAM influenced the system through periodicities of 23–30 d, affecting the intensity of the meridional wind field and the position of storm tracks over the southeast Pacific (Thompson and Woodworth, 2014; Pérez-Santos et al., 2019). Similarly, the MJO appeared to modulate the timing of renewal events at intraseasonal scales of 40–70 d (Jacques-Coper et al., 2015), potentially dictating the occurrence of the staircase-like sequences observed in highly ventilated years (Fig. 12). This teleconnection between tropical-extratropical variability and the deep Patagonian layer indicates that ventilation, along with being a local response to winter storms, is also a process conditioned by the broader state of circulation in the Southern Hemisphere (Ross et al., 2025). Spectral analysis supported this multi-scale interpretation, as the coherence between DO and wind forcing was the strongest in the bands corresponding to these climatic oscillators (Figs. 11 and 12). The shift in spectral energy observed between 2018 and 2022 indicates that the relative importance of these drivers changes through time, rendering the seasonal ventilation window a dynamic feature rather than a static annual occurrence. Ultimately, the interannual variability at the GM is the complex outcome of local synoptic events being steered by large-scale oscillators, which determine whether the fjord takes a short breath or achieves a sustained oxygenated state.

4.4 Implications for deoxygenation in northern Patagonia

The results of this study have direct implications for understanding deoxygenation in northern Patagonia and demonstrate that the oxygenation state at the GM depends on a dynamic equilibrium between two opposing processes. On one hand, the gateway serves as the primary conduit for the poleward advection of saline, oxygen-poor ESSW, which has demonstrated an increasing influence in recent years (Linford et al., 2023). On the other hand, it facilitates intermittent renewal of the deep

https://doi.org/10.5194/egusphere-2026-2329
Preprint. Discussion started: 5 May 2026

layer by subducting relatively oxygenated Subantarctic-derived waters during favourable synoptic events (Pérez-Santos et al., 2019). Consequently, the oxygen conditions observed at 170 m reflect the presence of deoxygenated source waters, as well as the time-varying balance between the import of hypoxic masses and the irregular efficiency of physical renewal. This interpretation refines the deoxygenation framework previously proposed for the region, where subsurface oxygen loss has been largely attributed to the progressive intensification of the ESSW (Linford et al., 2023; Linford et al., 2024). Although recent trends indicate a long-term decline in DO at the gateway, the present results suggest that this loss must also be interpreted through the lens of renewal efficiency. Deoxygenation at the fjord entrance is potentially exacerbated by a weakening of the physical buffering provided by winter ventilation. In practical terms, deep ventilation acts as an inherently discontinuous and unstable compensatory mechanism, as its success depends on the precise timing, persistence, and intensity of favourable atmospheric forcing (Narváez et al., 2019; Ross et al., 2025).

The distinction developed here between renewal events and oxygenated states is critical for assessing ecosystem resilience. Because a deep layer may retain oxygen inherited from a preceding ventilation episode, high DO values alone do not necessarily indicate active renewal (Keeling et al., 2010; Ayranci and Dashtgard, 2020). From a deoxygenation perspective, concentration metrics may overestimate the immediate status of the system, whereas mechanistic indicators such as AOU tendencies and thermohaline anomalies provide a more robust assessment of whether the deep layer is truly being refreshed (Sarmiento and Gruber, 2006). This differentiation is likely to become increasingly important in a warming ocean, where the duration of post-renewal persistence may shorten, even as occasional oxygenation events persist.

As the GM regulates the exchange between the open Pacific and inland basins, any shift in the renewal function at this boundary will likely propagate throughout the northern Patagonian fjord system. If the frequency or efficiency of deep ventilation declines owing to strengthening stratification or altered synoptic organization, the deep fjord basins will become increasingly exposed to the cumulative effects of imported low-oxygen waters without an effective compensating mechanism (Oschlies et al., 2018). Ultimately, deoxygenation in northern Patagonia is a potential reorganization of the balance between oxygen supply and consumption. Sustained observations at the GM are thus essential for tracking the progression of low-oxygen conditions as well as for determining whether the gateway is maintaining its capacity to buffer the inland sea against the ongoing climatic shift.

4.5 Limitations and perspectives

The reliance on a single fixed depth at 170 m provided a robust perspective on the temporal variability of deep oxygenation but constrained the characterization of the full vertical structure. Consequently, although the local expression of ventilation was well resolved, the three-dimensional renewal pathways and exact vertical extent of each event remained partially unconstrained. The observed thermohaline changes likely reflected complex mixtures and maritime intrusions reaching the measurement depth rather than direct replacement of the entire water column. This limitation is common in long-term Eulerian observations where the trade-off between temporal resolution and vertical coverage is inevitable (Nagano et al., 2016).

https://doi.org/10.5194/egusphere-2026-2329
Preprint. Discussion started: 5 May 2026

Furthermore, the forcing analysis relied primarily on wind-derived indices such as total Ekman forcing as proxies for downwelling- versus upwelling-favourable conditions. Although these metrics effectively identified the timing of atmospheric drivers, they did not fully represent the complex circulation at the GM. Recent research indicates that gateway exchange is strongly modulated by the nonlinear interaction between barotropic and baroclinic pressure gradients along with subtidal sea level variability (Ross et al., 2025). Therefore, the present results characterized the regional forcing context of ventilation without resolving the complete dynamical structure through which that forcing was translated into deep renewal at the fjord entrance.

The pulse and period framework was designed as a conservative operational tool to isolate the effective expression of ventilation at the mooring site. Although this approach allowed a clear distinction between sustained states and discrete events, it emphasized the local signal rather than the total magnitude of water-mass exchange across the gateway. Future studies integrating moored velocity measurements and high-resolution numerical modelling are thus essential to quantify the total oxygen flux entering the North Patagonian fjord system. Despite these constraints, the exceptional duration and resolution of the 2016 to 2024 time series constitute a major strength of this study. This record enabled the decoupling of recurrent seasonal patterns from synoptic extremes while distinguishing between active renewal and oxygenated persistence. This dataset provides a critical observational baseline for investigating deep renewal mechanisms under the current trend of global deoxygenation (Schmidtko et al., 2017; Breitburg et al., 2018). The distinction established between pulses and periods offers a mechanistic framework that is rarely available for fjord systems in the Southern Hemisphere.

Assessing how the renewal capacity of the GM evolves under increasing stratification and climatic variability should be a primary research priority. The results suggest that the efficiency of deep ventilation depends on the occurrence of favourable events as well as on the temporal organization of forcing and the thermohaline preconditioning of the gateway. Understanding whether these physical controls are reorganizing through time is essential to anticipate the future balance between oxygen consumption and supply in the Patagonian interior sea (Linford et al., 2023). In this context, sustained observations at the GM remain critical for determining whether this gateway can maintain its function as a buffer against the progression of hypoxic waters.

5. Conclusions

A time series of DO measurements from 2016 to 2024 at the deep layer (170 m) of a Patagonian fjord revealed that deep-water ventilation is an episodic phenomenon, mainly occurring seasonally from late winter to spring. Over the 9 year period, 16 ventilation events were identified, with an average duration of approximately 60 d each. Additionally, synoptic-scale oxygen supply events were characterized based on three criteria: (1) a rapid increase in DO, indicated by strongly negative trends in the rate of change of the AOU; (2) the oxygen increase lasting at least 2 d to distinguish real physical processes from noise; and (3) DO concentrations exceeding the hypoxia threshold during the event.

https://doi.org/10.5194/egusphere-2026-2329
Preprint. Discussion started: 5 May 2026

Downwelling-favourable winds were identified as the main drivers of prolonged ventilation periods, pushing oxygen-rich surface waters into deeper layers. Additionally, salinity decreases were observed before and during ventilation events, which enhanced oxygen solubility. In contrast, the water temperature did not appear to enhance ventilation. On the interannual scale, 2016 and 2017 experienced one of the most extensive and intense deep-water ventilation periods, primarily driven by the "El Niño 2015–2016" event. This event led to strong downwelling-favourable winds, which enhanced the injection of oxygenated surface waters into the bottom waters as well as deepened the poorly oxygenated ESSW mass. This process enabled the entry of well-oxygenated SAAW into the Patagonian fjords, further supporting deep-water ventilation. In 2017, the deep-water ventilation period was, once again, primarily attributed to stronger downwelling-favourable winds. However, the specific processes contributing to the observed increase in DO during this period remain unexplored and warrant further investigation. Wavelet and coherence analyses indicated that the dominant timescales of oxygen variability and strength of atmospheric coupling changed through time. This suggests that ventilation efficiency is modulated by large-scale temporal climate modes, such as the BAM or MJO, which regulate the frequency of synoptic triggers.

In total, 35 ventilation pulses were identified, with most occurring within the broader ventilation periods. Analysis of these pulses demonstrated that renewal events were consistently preceded by increasingly negative total Ekman transport forcing and northern wind stress, followed by a lagged increase in oxygen levels and concurrent thermohaline changes. This sequence highlights synoptic downwelling-favourable forcing as the primary trigger for deep-water renewal. However, persistence of the resulting oxygenated conditions depended on whether the events occurred within a favourable seasonal background and whether they were sufficiently recurrent to allow oxygen accumulation before respiratory depletion resumed.

Ultimately, the GM functions as a dynamic gateway, where episodic renewal intermittently counteracts the long-term influence of low-oxygen subsurface waters entering northern Patagonia. In this context, regional deoxygenation should be understood as a trend of declining oxygen content as well as a possible weakening of the renewal processes that temporarily offset that trend. As this gateway regulates exchange between the open Pacific Ocean and inland sea, any reduction in the frequency or efficiency of deep ventilation can diminish the capacity of the fjords to buffer ongoing oxygen loss. Consequently, sustained long-term observations at the GM are essential for detecting changes in renewal dynamics and for anticipating the physical and biogeochemical consequences of deoxygenation in the Patagonian fjord system.

Author contributions

CSH and IPS: led the study design, data collection, analysis of physical oceanographic data, and manuscript writing. MC: analysis of wind data, and manuscript revision. MC: manuscript revision. AB: statistical analysis, MCA: analysis of synoptic events. All authors contributed to the writing of the present manuscript.

https://doi.org/10.5194/egusphere-2026-2329
Preprint. Discussion started: 5 May 2026

Conflict of interest

The authors declare that they have no conflict of interest relevant to this study.

Acknowledgments

We thank the crew of the Don Felipe III for their invaluable support during data collection. Special thanks are extended to the students and technicians for facilitating the data collection.

Financial support

Iván Pérez-Santos was supported by FONDECYT 1211037, 1251038, and COPAS COASTAL FB210021.

Data Availability Statement

Iván Pérez-Santos. (2026). Time series of temperature, salinity, oxygen, and Ekman derived variables in period 2016-2014, Patagonian Fjords [Data set]. Zenodo. https://doi.org/10.5281/zenodo.19711029

References

Aguirre, C., Pizarro, Ó., Strub, P. T., Garreaud, R., and Barth, J. A.: Seasonal dynamics of the near-surface alongshore flow off central Chile, J. Geophys. Res.-Oceans, 117, C01006, https://doi.org/10.1029/2011JC007379, 2012.

Akaike, H.: A new look at the statistical model identification, IEEE Trans. Autom. Control, 19, 716–723, https://doi.org/10.1109/TAC.1974.1100705, 1974.

Ayranci, K. and Dashtgard, S. E.: Deep-water renewal events; insights into deep water sediment transport mechanisms, Earth-Sci. Rev., 203, 103138, 2020.

Bell, B., Hersbach, H., Berrisford, P., Dahlgren, P., Horányi, A., Muñoz Sabater, J., Nicolas, J., Radu, R., Schepers, D., Simmons, A., Soci, C., Vamborg, S., and Thépaut, J.-N.: ERA5 hourly data on single levels from 1950 to 1978 (preliminary version), Copernicus Climate Change Service (C3S) Climate Data Store (CDS) [data set], https://doi.org/10.24381/cds.f1705039, 2020.

Belzile, M., Galbraith, P. S., and Bourgault, D.: Water renewals in the Saguenay Fjord, J. Geophys. Res. Oceans, 121, 638–657, https://doi.org/10.1002/2015JC011085, 2016.

https://doi.org/10.5194/egusphere-2026-2329
Preprint. Discussion started: 5 May 2026

Bertrand, J. C., Bonin, P., Caumette, P., Gattuso, J. P., Grégori, G., Guyoneaud, R., and Poly, F.: Biogeochemical cycles, in: Environmental Microbiology: Fundamentals and Applications: Microbial Ecology, 511–617, 2015.

Bianchi, T. S., Arndt, S., Austin, W. E., Benn, D. I., Bertrand, S., Cui, X., et al.: Fjords as aquatic critical zones (ACZs), Earth-Sci. Rev., 203, 103145, https://doi.org/10.1016/j.earscirev.2020.103145, 2020.

Breitburg, D., Levin, L. A., Oschlies, A., Grégoire, M., Chavez, F. P., Conley, D. J., et al.: Declining oxygen in the global ocean and coastal waters, Science, 359, eaam7240, 2018.

Buchan, S. J., Pérez-Santos, I., Narváez, D., Castro, L., Stafford, K. M., Baumgartner, M. F., et al.: Intraseasonal variation in southeast Pacific blue whale acoustic presence, zooplankton backscatter, and oceanographic variables on a feeding ground in Northern Chilean Patagonia, Prog. Oceanogr., 199, 102709, 2021.

Crawford, D. W., Montero, P., and Daneri, G.: Blooms of Alexandrium catenella in coastal waters of Chilean Patagonia: Is Subantarctic Surface Water involved?, Front. Mar. Sci., 8, 612628, https://doi.org/10.3389/fmars.2021.612628, 2021.

de Boer, A. M., Sigman, D. M., Toggweiler, J. R., and Russell, J. L.: Effect of global ocean temperature change on deep ocean ventilation, Paleoceanography, 22, PA2210, https://doi.org/10.1029/2005PA001242, 2007.

Crawley, M. J.: The R Book, John Wiley & Sons Ltd, West Sussex, UK, 942 pp., 2007

Font, E., Swart, S., Bruss, G., Sheehan, P. M. F., Heywood, K. J., and Queste, B. Y.: Ventilation of the Arabian Sea oxygen minimum zone by Persian Gulf Water, J. Geophys. Res. Oceans, 129, e2023JC020668, https://doi.org/10.1029/2023JC020668, 2024.

Fox, J., Weisberg, S., 2010. An R companion to applied regression. Sage, Thousand Oaks.

Fuenzalida, R., Schneider, W., Garcés-Vargas, J., Bravo, L., and Lange, C.: Vertical and horizontal extension of the oxygen minimum zone in the Eastern South Pacific Ocean, Deep-Sea Res. Pt. II, 56, 1027–1038, https://doi.org/10.1016/j.dsr2.2008.11.001, 2009.

Garreaud, R. D., Vuille, M., Compagnucci, R., and Marengo, J.: Present-day South American climate, Palaeogeogr. Palaeoclimatol. Palaeoecol., 281, 180–195, https://doi.org/10.1016/j.palaeo.2007.10.032, 2009.

https://doi.org/10.5194/egusphere-2026-2329
Preprint. Discussion started: 5 May 2026

Garcia-Santos, Y., Narvaez, D. A., Jacques-Coper, M., Saldias, G. S., Bozkurt, D., & Alessio, B. M. Dominant wind patterns under the influence of atmospheric rivers: Implications for coastal upwelling off central-southern Chile. Journal of Geophysical Research: Oceans, 130,e2024JC021444. https://doi.org/10.1029/2024JC021444, 2025a.

García-Santos, Y., Narváez, D.A., Saldías, G.S. et al. Impact of atmospheric rivers on coastal oceanographic conditions off central-southern Chile. Sci Rep 15, 34569, https://doi.org/10.1038/s41598-025-17997-w, 2025b.

Gotelli, N.J., Ellison, A.M., 2004. A primer of ecological statistics. Vol. 1. Sunderland: Sinauer Associates Publishers.

Gruber, N.: Warming up, turning sour, losing breath: ocean biogeochemistry under global change, Philos. T. R. Soc. A, 369, 1980–1996, 2011.

Hamme, R. C., Berry, J. E., and Klymak, J. M.: In situ O2 and N2 measurements detect deep-water renewal dynamics in seasonally anoxic Saanich Inlet, Cont. Shelf Res., 110, 140–147, 2015.

Hannah, C. G., Johannessen, S. C., Wright, C. A., and Page, S. J.: Oxygen dynamics in a deep-silled fjord: Tight coupling to the open shelf, Limnol. Oceanogr., 69, 652–666, https://doi.org/10.1002/lno.12522, 2024.

Henley, B. J., Gergis, J., Karoly, D. J., Power, S. B., Kennedy, J., and Folland, C. K.: A tripole index for the interdecadal Pacific oscillation, Clim. Dynam., 45, 3077–3090, https://doi.org/10.1007/s00382-015-2525-1, 2015.

Hobday, A. J., Alexander, L. V., Perkins, S. E., Smale, D. A., Straub, S. C., Oliver, E. C., Benthuysen, J. A., Burrows, M. T., Donat, M. G., Holbrook, N. J., Moore, P. J., Scannell, H. A., Gupta, A. S., and Wernberg, T.: A hierarchical approach to defining marine heatwaves, Prog. Oceanogr., 141, 227–238, https://doi.org/10.1016/j.pocean.2015.12.014, 2016.

Hormazábal, S., Shaffer, G., Silva, N., and Navarro, E.: La corriente subsuperficial del Perú-Chile y la variabilidad de la zona de mínimo oxígeno frente a Chile central, Gayana, 70, 37–45, https://doi.org/10.4067/S0717-65382006000300009, 2006.

Iriarte, J. L., Pantoja, S., and Daneri, G.: Oceanographic processes in Chilean fjords of Patagonia: from small to large-scale studies, Prog. Oceanogr., 129, 1–7, 2014.

https://doi.org/10.5194/egusphere-2026-2329
Preprint. Discussion started: 5 May 2026

Jackson, J. M., Thomson, R. E., Brown, L. N., Willis, P. G., and Borstad, G. A.: Satellite chlorophyll off the British Columbia coast, 1997–2010, J. Geophys. Res. Oceans, 120, 4709–4728, https://doi.org/10.1002/2014JC010496, 2015.

Jackson, J. M., Johannessen, S. C., Del Bel Belluz, J., Hunt, B. P. V., and Hannah, C. G.: Identification of a seasonal subsurface oxygen minimum in Rivers Inlet, British Columbia, Estuaries Coasts, 45, 754–771, https://doi.org/10.1007/s12237-021-00999-y, 2022.

Jackson, J. M., Hare, A., Hannah, C. G., Hilborn, A., Zahner, V., Page, S. J., Rosen, S., Timmerman, V., and Lee, A. H.: Why Deep-Water Dissolved Oxygen Is Higher in Gandaawuu.Ngaay Xyangs (Juan Perez Sound), Haida Gwaii, Than Other British Columbia Fjords, J. Geophys. Res. Oceans, 130, e2024JC021826, https://doi.org/10.1029/2024JC021826, 2025.

Jacox, M. G., Edwards, C. A., Hazen, E. L., and Bograd, S. J.: Coastal upwelling revisited: Ekman, Bakun, and improved upwelling indices for the U.S. West Coast, J. Geophys. Res. Oceans, 123, 7332–7350, https://doi.org/10.1029/2018JC014187, 2018.

Jacques-Coper, M., S. Brönnimann, O. Martius, C. S. Vera, and S. B. Cerne. Evidence for a modulation of the intraseasonal summer temperature in Eastern Patagonia by the Madden-Julian Oscillation, J. Geophys. Res. Atmos., 120, 7340–7357, doi:10.1002/2014JD022924, 2015.

Keeling, R. F., Körtzinger, A., and Gruber, N.: Ocean deoxygenation in a warming world, Annu. Rev. Mar. Sci., 2, 199–229, 2010.

Klymak, J. M., Jackson, J. M., and Hannah, C. G.: Predicting Upwelling due to Down-Fjord Winds, J. Phys. Oceanogr., 55, e2024JPO0176, https://doi.org/10.1175/JPO-D-24-0176.1, 2025.

Leth, O., Shaffer, G., and Ulloa, O.: Hydrography of the eastern South Pacific Ocean: Results from the Sonne 102 cruise, May–June 1995, Deep-Sea Res. Pt. II, 51, 2349–2369, https://doi.org/10.1016/j.dsr2.2004.08.009, 2004.

Levin, L. A., Bett, B. J., Gates, A. R., Heimbach, P., Howe, B. M., Janssen, F., et al.: Global observing needs in the deep ocean, Front. Mar. Sci., 6, 241, 2019.

Leys, C., Ley, C., Klein, O., Bernard, P., and Licata, L.: Detecting outliers: Do not use standard deviation around the mean, use absolute deviation around the median, J. Exp. Soc. Psychol., 49, 764–766, https://doi.org/10.1016/j.jesp.2013.03.013, 2013.

https://doi.org/10.5194/egusphere-2026-2329
Preprint. Discussion started: 5 May 2026

Linford, P., Pérez-Santos, I., Montes, I., Dewitte, B., Buchan, S., Narváez, D., et al.: Recent deoxygenation of Patagonian fjord subsurface waters connected to the Peru–Chile Undercurrent and Equatorial Subsurface Water variability, Global Biogeochem. Cy., 37, e2022GB007688, 2023.

Linford, P., Pérez-Santos, I., Montero, P., Díaz, P. A., Aracena, C., Pinilla, E., et al.: Oceanographic processes driving low-oxygen conditions inside Patagonian fjords, Biogeosciences, 21, 1433–1459, https://doi.org/10.5194/bg-21-1433-2024.

Long, M. C., Deutsch, C., and Ito, T.: Finding forced trends in oceanic oxygen, Global Biogeochem. Cy., 30, 381–397, https://doi.org/10.1002/2015GB005310, 2016.

MacGilchrist, G. A., Marshall, D. P., Johnson, H. L., Lique, C., and Thomas, M.: Characterizing the chaotic nature of ocean ventilation, J. Geophys. Res. Oceans, 122, 7577–7594, https://doi.org/10.1002/2017JC012875, 2017.

Marcotte, D.: Cokriging with MATLAB, Comput. Geosci., 17, 1265–1280, https://doi.org/10.1016/0098-3004(91)90028-C, 1991.

McCullagh, P. and Nelder, J. A.: Generalized Linear Models, 2nd edn., Chapman and Hall, London, UK, 511 pp., 1989.

McDougall, T. J., Feistel, R., Millero, F. J., Jackett, D. R., Wright, D. G., King, B. A., et al.: The international thermodynamic equation of seawater 2010 (TEOS-10): Calculation and use of thermodynamic properties, IOCCP Rep., 14, 2009.

Moffat, C.: Wind-driven modulation of warm supply to a proglacial fjord, Jorge Montt Glacier, Patagonia, Geophys. Res. Lett., 41, 3943–3950, https://doi.org/10.1002/2014GL060023, 2014.

Montes, I., Colas, F., Capet, X., and Schneider, W.: On the pathways of the equatorial subsurface currents in the eastern equatorial Pacific and their contributions to the Peru-Chile Undercurrent, J. Geophys. Res.-Oceans, 115, C09003, https://doi.org/10.1029/2009JC005710, 2010.

Nagano, A., Yamashita, S., Hasegawa, K., Ariyoshi, K., and Kawaguchi, K.: Spatial distribution of dissolved oxygen and its variation on the North Pacific subtropical mode water in the vicinity of the Izu-Ogasawara Ridge, J. Oceanogr., 72, 853–864, https://doi.org/10.1007/s10872-016-0386-9, 2016.

Narváez, D. A., Vargas, C. A., Cuevas, L. A., García-Loyola, S. A., Lara, C., Segura, C., et al.: Dominant scales of subtidal variability in coastal hydrography of the Northern Chilean Patagonia, J. Mar. Syst., 193, 59–73, https://doi.org/10.1016/j.jmarsys.2018.12.008, 2019.

Naveira Garabato, A. C., MacGilchrist, G. A., Brown, P. J., Evans, D. G., Meijers, A. J., and Zika, J. D.: High-latitude ocean ventilation and its role in Earth's climate transitions, Philos. T. R. Soc. A, 375, 20160324, 2017.

Oschlies, A., Brandt, P., Stramma, L., and Schmidtko, S.: Drivers and mechanisms of ocean deoxygenation, Nat. Geosci., 11, 467–473, 2018.

Palter, J. B., Frölicher, T. L., Paynter, D., and John, J. G.: Climate, ocean circulation, and sea level changes under stabilization and overshoot pathways to 1.5 K warming, Earth Syst. Dynam., 9, 817–828, 2018.

Paulmier, A. and Ruiz-Pino, D.: Oxygen minimum zones (OMZs) in the modern ocean, Progr. Oceanogr., 80, 113–128, https://doi.org/10.1016/j.pocean.2008.08.001, 2009.

Pérez-Santos, I., Garcés-Vargas, J., Schneider, W., Ross, L., Parra, S., and Valle-Levinson, A.: Double-diffusive layering and mixing in Patagonian fjords, Prog. Oceanogr., 129, 35–49, https://doi.org/10.1016/j.pocean.2014.03.012, 2014.

Pérez-Santos, I., Garcés-Vargas, J., Schneider, W., Ross, L., Parra, S., and Pérez-Hernández, M. D.: Spatiotemporal variability of the oxygen minimum zone off the Chilean coast (2012–2015), Sci. Total Environ., 537, 129–138, https://doi.org/10.1016/j.scitotenv.2015.07.160, 2015

Pérez-Santos, I.: Deep ventilation event during fall and winter 2015 in the Puyuhuapi Fjord (44.6°S), Lat. Am. J. Aquat. Res., 45, 223–227, https://doi.org/10.3856/vol45-issue1-fulltext-25, 2017.

Pérez-Santos, I., Castro, L., Ross, L., Niklitschek, E., Mayorga, N., Cubillos, L., et al.: Turbulence and hypoxia contribute to the formation of dense biological scattering layers in a Patagonian fjord system, Ocean Sci., 14, 1185–1206, https://doi.org/10.5194/os-14-1185-2018.

Pérez-Santos, I., Seguel, R., Schneider, W., Linford, P., Donoso, D., Navarro, E., et al.: Synoptic-scale variability of surface winds and ocean response to atmospheric forcing in the eastern austral Pacific Ocean, Ocean Sci., 15, 1247–1266, https://doi.org/10.5194/os-15-1247-2019.

Pérez-Santos, I.: Time series of temperature, salinity, oxygen, and Ekman derived variables in period 2016-2014, Patagonian Fjords [Data set]. Zenodo. https://doi.org/10.5281/zenodo.19711029, 2026.

Pinilla, E., Castillo, M. I., Pérez-Santos, I., Venegas, O., and Valle-Levinson, A.: Water age variability in a Patagonian fjord, J. Mar. Syst., 210, 103376, https://doi.org/10.1016/j.jmarsys.2020.103376, 2020.

Pond, S. and Pickard, G. L.: Introductory Dynamical Oceanography, 2nd edn., Gulf Professional Publishing, 329 pp., 1983.

R Core Team: R: A language and environment for statistical computing, R Foundation for Statistical Computing, Vienna, Austria, available at: https://www.R-project.org/ (last access: 22 April 2026), 2019.

Radko, T.: Double-diffusive Convection, Cambridge University Press, Cambridge, 2013.

Rahn, D. A. and Garreaud, R. D.: A synoptic climatology of the near-surface wind along the west coast of South America, Int. J. Climatol., 34, 780–792, https://doi.org/10.1002/joc.3724, 2014.

Rhein, M., Steinfeldt, R., Kieke, D., Stendardo, I., and Yashayaev, I.: Ventilation variability of Labrador Sea Water and its impact on oxygen and anthropogenic carbon: a review, Philos. T. R. Soc. A, 375, 20160321, 2017.

Ross, L., Pérez-Santos, I., Linford, P., and Díaz, P. A.: Circulation in the Guafo Mouth: The gateway to northern Patagonia, Sci. Total Environ., 979, 179512, https://doi.org/10.1016/j.scitotenv.2025.179512, 2025.

R Core Team: R: A language and environment for statistical computing, R Foundation for Statistical Computing, Vienna, Austria, available at: https://www.R-project.org/ (last access: 22 April 2026), 2019.

Sagen, T. S., Asplin, L., Darelius, E., Johnsen, I. A., and Myksvoll, M. S.: Observations and modeling of the 2021 deep-water renewal event in Masfjorden, a sill fjord in Western Norway, Estuar. Coast. Shelf Sci., 312, 108920, 2025.

Saldías, G. S., Sobarzo, M., and Quiñones, R.: Freshwater structure and its seasonal variability off Western Patagonia, Prog. Oceanogr., 174, 143–153, https://doi.org/10.1016/j.pocean.2018.10.014, 2019.

Sarmiento, J. L. and Gruber, N.: Ocean Biogeochemical Dynamics, Princeton University Press, Princeton, USA, 526 pp., 2006.

https://doi.org/10.5194/egusphere-2026-2329
Preprint. Discussion started: 5 May 2026

Schmidtko, S., Stramma, L., and Visbeck, M.: Decline in global oceanic oxygen content during the past five decades, Nature, 542, 335–339, 2017.

Schneider, W., Pérez-Santos, I., Ross, L., Bravo, L., Seguel, R., and Hernández, F.: On the hydrography of Puyuhuapi Channel, Chilean Patagonia, Prog. Oceanogr., 129, 8–18, https://doi.org/10.1016/j.pocean.2014.03.007, 2014.

Schneider, W., Donoso, D., Garcés-Vargas, J., and Escribano, R.: Water-column cooling and sea surface salinity increase in the upwelling region off central-south Chile driven by a poleward displacement of the South Pacific High, Prog. Oceanogr., 151, 38–48, https://doi.org/10.1016/j.pocean.2016.11.004, 2017.

Shepherd, J. G., Brewer, P. G., Oschlies, A., and Watson, A. J.: Ocean ventilation and deoxygenation in a warming world: introduction and overview, Philos. T. R. Soc. A, 375, 20170240, 2017.

Sievers, H.: Temperature and salinity in the austral Chilean channels and fjords, in: Progress in the Oceanographic Knowledge of Chilean Interior Waters, from Puerto Montt to Cape Horn, edited by: Silva, N. and Palma, S., Comité Oceanográfico Nacional–Pontificia Universidad Católica de Valparaíso, Valparaíso, 31–36, 2008.

Sievers, A. H. and Silva, N.: Water masses and circulation in austral Chilean channels and fjords, in: Progress in the Oceanographic Knowledge of Chilean Inner Waters, from Puerto Montt to Cape Horn, edited by: Silva, N. and Palma, S., Comité Oceanográfico Nacional–Pontificia Universidad Católica de Valparaíso, Valparaíso, 53–58, 2008.

Silva, N. and Vargas, C. A.: Hypoxia in Chilean Patagonian fjords, Prog. Oceanogr., 129, 62–74, https://doi.org/10.1016/j.pocean.2014.05.016, 2014.

Silva, N., Rojas, N., and Fedele, A.: Water masses in the Humboldt Current System: Properties, distribution, and the nitrate deficit as a chemical water mass tracer for Equatorial Subsurface Water off Chile, Deep-Sea Res. Pt. II, 56, 1004–1020, https://doi.org/10.1016/j.dsr2.2008.12.013, 2009.

Smith, R. L.: Upwelling, Oceanogr. Mar. Biol. Annu. Rev., 6, 11–46, 1968.

Stommel, H.: Determination of water mass properties of water pumped down from the Ekman layer to the geostrophic flow below, Proc. Natl. Acad. Sci. USA, 76, 3051–3055, 1979.

Talley, L. D.: Descriptive Physical Oceanography: An Introduction, Academic Press, 2011.

https://doi.org/10.5194/egusphere-2026-2329
Preprint. Discussion started: 5 May 2026

Torrence, C. and Compo, G. P.: A practical guide to wavelet analysis, Bull. Amer. Meteor. Soc., 79, 61–78, https://doi.org/10.1175/1520-0477(1998)079<0061:APGTWA>2.0.CO;2, 1998.

Thompson, D. W. J. and Woodworth, J. D.: Barotropic and baroclinic annular variability in the southern hemisphere, J. Atmos. Sci., 71, 1480–1493, https://doi.org/10.1175/JAS-D-13-0185.1, 2014.

Venables, W. N. and Ripley, B. D.: Modern Applied Statistics with S-PLUS, 4th edn., Springer Science & Business Media, New York, USA, 495 pp., 2013.

Yelland, M. and Taylor, P. K.: Wind stress measurements from the open ocean, J. Phys. Oceanogr., 26, 541–558, https://doi.org/10.1175/1520-0485(1996)026<0541:WSMFTO>2.0.CO;2, 1996.

Yamamoto, A., Abe-Ouchi, A., Shigemitsu, M., Oka, A., Takahashi, K., Ohgaito, R., and Yamanaka, Y.: Global deep ocean oxygenation by enhanced ventilation in the Southern Ocean under long-term global warming, Global Biogeochem. Cy., 29, 1801–1815, 2015.

Zhang, J., Gilbert, D., Gooday, A. J., Levin, L., Naqvi, S. W. A., Middelburg, J. J., et al.: Natural and human-induced hypoxia and consequences for coastal areas: synthesis and future development, Biogeosciences, 7, 1443–1467, 2010.